A NOVEL APPROACH TO THE RENDEZVOUS PROBLEM FOR AERIAL REFUELING OF MULTI-UAV SYSTEMS

by
AHMET FARUK GÜNALP

Submitted to the Graduate School of Engineering and Natural Sciences
in partial fulfilment of
the requirements for the degree of Master of Science

Sabancı University
July 2025

A NOVEL APPROACH TO THE RENDEZVOUS PROBLEM FOR REFUELING OF MULTI-UAV SYSTEMS

Approved by:

Prof. MUSTAFA ÜNEL .....
(Thesis Supervisor)

Asst. Prof. MELİH TÜRKSEVEN .....

Asst. Prof. ABDURRAHMAN ERAY BARAN .....

Date of Approval: June 27, 2025

ABSTRACT

A NOVEL APPROACH TO THE RENDEZVOUS PROBLEM FOR AERIAL REFUELING OF MULTI-UAV SYSTEMS

AHMET FARUK GÜNALP

Mechatronics Engineering M.Sc. Thesis, July 2025

Thesis Supervisor: Prof. MUSTAFA ÜNEL

Keywords: aerial refueling, rendezvous problem, formation control, distributed control, multi UAV systems

Advancements in unmanned aerial vehicle (UAV) technology have led to their widespread adoption in both industry and academia. In recent years, the increasing focus on multi-agent systems has brought UAVs further into the spotlight. Multiple UAVs can perform tasks that are beyond the capabilities of a single vehicle or execute shared missions with enhanced efficiency and effectiveness. Aerial refueling, a strategic and long-established procedure in both civil and military aviation, significantly extends the range and operational capabilities of aerial vehicles. Recent research has explored automating this process for both manned and unmanned aircraft; however, current efforts primarily address single-vehicle scenarios. Given the growing use of UAV swarms in applications such as search and rescue, terrain map ping, and disaster relief, autonomous aerial refueling for multiple UAVs represents a logical and necessary next step. This thesis addresses the rendezvous problem for multiple UAVs approaching a tanker aircraft. Reference trajectories are generated using virtual spring-damper and charged particle models. A distributed control architecture is designed, employing waypoint-following controllers for individual vehicles. In 2D proof-of-concept scenarios, non-holonomic UGVs are utilized, and their motion control is achieved via cascaded controllers which utilize virtual inputs. Additionally, a novel collision avoidance algorithm and a two-phase docking procedure are proposed. To validate the proposed framework, a series of coordinated task scenarios involving groups of UGVs and UAVs are simulated in both 2D and 3D environments. The results confirm the effectiveness of the coordination strategy and formation control, demonstrating robust and satisfactory performance across a variety of scenarios.

ÖZET

ÇOKLU İHA SISTEMLERININ HAVADA YAKIT İKMALI IÇIN BULUŞMA PROBLEMINE YENI BIR YAKLAŞIM

AHMET FARUK GÜNALP

Mekatronik Mühendisliği Yüksek Lisans Tezi, Temmuz 2025

Tez Danışmanı: Prof. Dr. MUSTAFA ÜNEL

Anahtar Kelimeler: havada yakıt ikmali, buluşma problemi, formasyon kontrolü, dağıtımlı kontrol, çoklu İHA sistemleri

İnsansız hava aracı (İHA) teknolojisindeki gelişmeler, bu araçların hem sanayide hem de akademide yaygın olarak benimsenmesine yol açmıştır. Son yıllarda çok ajanlı sistemlere artan ilgi, İHA'ları daha da ön plana çıkarmıştır. Birden fazla İHA, tek bir aracın kapasitesini aşan görevleri yerine getirebilir veya ortak görevleri daha yüksek verimlilik ve etkinlikle icra edebilir.

Sivil ve askeri havacılıkta uzun süredir uygulanan stratejik bir prosedür olan havadan yakıt ikmali, hava araçlarının menzilini ve operasyonel yeteneklerini önemli ölçüde artırır. Son araştırmalar, bu sürecin hem insanlı hem de insansız hava araçları için otomatikleştirilmesini incelemiştir; ancak mevcut çalışmalar genellikle tek araçlı senaryoları ele almaktadır. Arama kurtarma, arazi haritalama ve afet yardımı gibi uygulamalarda İHA sürülerinin kullanımının artmasıyla, çoklu İHA'lar için otonom havadan yakıt ikmali mantıklı ve gerekli bir sonraki adım olarak ortaya çıkmaktadır.

Bu tez, bir tanker uçağa yaklaşan çoklu İHA'ların buluşma (randevu) problemini ele almaktadır. Referans yörüngeleri, sanal yay-sönümleyici ve yüklü parçacık modelleri kullanılarak oluşturulmuştur. Bireysel araçlar için yol noktası takibi yapan denetleyicilerin kullanıldığı dağıtık bir kontrol mimarisi tasarlanmıştır. 2B kavramsal kanıt senaryolarında, insansız kara araçları (İKA) kullanılmış ve bu araçların hareket kontrolleri, sanal girişler kullanan katmanlı denetleyiciler aracılığıyla sağlanmıştır. Ayrıca, yeni bir çarpışma önleme algoritması ve iki aşamalı bir kenetlenme prosedürü önerilmiştir. Önerilen çerçeveyi doğrulamak amacıyla, hem 2B hem de 3B ortamlarda İKA ve İHA gruplarını içeren koordineli görev senaryoları simüle edilmiştir. Elde edilen sonuçlar, koordinasyon stratejisinin ve formasyon kontrolünün etkinliğini doğrulamış, çeşitli senaryolarda sağlam ve tatmin edici performans sergilemiştir.

ACKNOWLEDGEMENTS

First and foremost, I would like to express my deepest gratitude to my supervisor, Prof. Dr. Mustafa Ünel, for his patience, invaluable guidance, expertise, and unwavering support. His encouragement and high standards consistently pushed me to strive for excellence, ultimately leading to the successful completion of this dissertation.

I would like to extend my sincere gratitude to my thesis committee members, Asst. Prof. Dr. Melih Türkseven and Asst. Prof. Dr. Abdurrahman Eray Baran, for their interest in my research and their insightful feedback, which greatly contributed to the development of this work.

I am also sincerely thankful to my lab mates, with whom I shared countless meaningful moments throughout our academic journey. I am especially grateful to Abdulmouti and my roommate, İlhami Osman, for their continuous help, inspiration, and support during our research years.

Last but certainly not least, I would like to thank my family. To my parents—thank you for raising me with such care, for your constant guidance, and for your wholehearted support at every stage of my life. I am also grateful to my brother, Yusuf Kerem, for his assistance with the illustrations; his support brought me much-needed peace of mind during challenging times.

To my family...

TABLE OF CONTENTS

LIST OF TABLES

LIST OF FIGURES

1. INTRODUCTION

Unmanned Aerial Vehicles (UAVs), commonly referred to as drones, are aircraft systems operated without an onboard human pilot, relying instead on remote control or autonomous flight capabilities. Originating as rudimentary remotely piloted vehicles in the early 20th century (Cook, 2007), UAVs have evolved dramatically in both design and functionality, particularly over the past few decades. Initially developed for military reconnaissance (Sullivan, 2006) and target practice, they are now employed across a wide range of sectors, including agriculture, environmental monitoring, disaster response, logistics, filmmaking, and law enforcement (Samad, Kamarulzaman, Hamdani, Mastor & Hashim, 2013). UAVs are classified into several types based on size, range, and function—ranging from small consumer drones to large-scale military platforms capable of long-endurance missions (Mishra, Yadav, Rath & Kumar, 2024).

The rising popularity of UAVs can be attributed to their numerous advantages: they reduce human risk in hazardous environments, lower operational costs, provide real-time data, and can access areas that are difficult or dangerous for manned aircraft. These features make UAVs highly attractive for both civilian and defense applications. In practice, UAVs are utilized for aerial surveillance, precision agriculture, infrastructure inspection, delivery services, and tactical military operations, among many other purposes (Cai, Lum, Chen & Lee, 2010). As technological advancements continue to enhance their autonomy, payload capacity, and communication systems, UAVs are poised to play an increasingly vital role in both commercial and strategic domains (Zhou, Rao & Wang, 2020).

Multi-Unmanned Aerial Vehicle (multi-UAV) systems represent a significant evolution in unmanned flight operations, enabling the coordinated deployment of multiple UAVs to perform complex, large-scale, or distributed tasks. The concept of using multiple drones in a synchronized manner has gained momentum due to the limitations of single-UAV operations, particularly in missions requiring broad spatial coverage, redundancy, or simultaneous actions. Driven by advances in autonomous control, swarm intelligence, and wireless communication, multi-UAV systems have

transitioned from experimental research to real-world applications in both military and civilian domains. Some of the popular UAVs are shown in Fig. 1.1

(a) (b) (c)

Figure 1.1 Well-known UAVs (images courtesy of BAYKAR and TAI)
a) Bayraktar Akıncı b) TAI Anka) c) Bayraktar TB-2

Historically, early efforts in multi-UAV coordination emerged within defense research programs seeking to improve battlefield surveillance and target tracking. Today, a wide range of multi-UAV configurations exist—from loosely coordinated fleets to tightly integrated autonomous swarms—each tailored to specific operational needs (Xiaoning, 2020). Prominent projects and systems include military reconnaissance swarms, collaborative mapping missions, and disaster response fleets that communicate and adapt in real time. These systems are increasingly utilized in areas such as environmental monitoring, infrastructure inspection, search and rescue, precision agriculture, and security patrols.

The advantages of multi-UAV systems are substantial. They offer enhanced efficiency, scalability, and mission resilience; the ability to cover more ground in less time; and increased robustness in the event of individual UAV failure. Additionally, cooperative behaviors among drones enable complex task division, real-time data fusion, and adaptive decision-making, which are essential in dynamic or uncertain environments (Ding, Rahmani & Egerstedt, 2010). As research in swarm algorithms and distributed control continues to advance, multi-UAV systems are set to redefine the possibilities of autonomous aerial operations across a wide spectrum of fields (Zhang, Yan & Zhang, 2020).

Coordinated motion and formation control in Unmanned Aerial Vehicle (UAV) systems are central to the successful deployment of multi-UAV operations, particularly in missions requiring precision, efficiency, and real-time adaptability. Formation control refers to the ability of multiple UAVs to move cohesively in predefined geometric patterns while maintaining safe inter-vehicle distances, consistent velocity, and synchronized navigation. This capability is essential in applications such as surveillance, environmental mapping, wireless communication relays, and military tactics, where organized spatial arrangement significantly enhances performance and

data coverage. Fig. 1.2 shows a fighter jet squadron on a mission, it is common to see them refuel sequentially.

Figure 1.2 Multiple aircraft are used for various operations (on a Novel Back-Stepping Approach, mul)

Developing reliable UAV coordination strategies (Martínez, Richardson, Thomas, du Bois & Campoy, 2013; Muslimov & Munasypov, 2021; Wu, Wang & Qi, 2022) involves complex control architectures that can manage decentralized decision-making, dynamic reconfiguration, and environmental uncertainty (Duan, Yuan & Zeng, 2022). Techniques for formation control like in Fig. 1.3 range from leader–follower models and behavior-based algorithms to consensus and artificial potential field approaches, each offering specific trade-offs in responsiveness, stability, and scalability (Hao & Quan, 2021; Jaiswal & Vashisth, 2023). Despite significant progress, several key challenges persist. These include maintaining communication integrity among UAVs, avoiding inter-vehicle collisions, managing energy efficiency, and adapting to unpredictable environmental disturbances such as wind, terrain, or signal interference (Fang, Yao, Zhu & Chen, 2023; Ouyang, Wu, Cong & Wang, 2023).

Moreover, the integration of real-time sensing, obstacle avoidance, and fault tolerance remains an ongoing research focus (Muskardin, Coelho, Noce, Ollero & Kondak, 2020). As UAV swarms become increasingly autonomous, ensuring coordinated motion in contested or cluttered airspaces demands robust control systems that are both flexible and resilient (PS, 2020). Addressing these challenges is critical to unlocking the full potential of UAV teams in both civilian and defense-oriented missions (Cao, Yu, Ren & Chen, 2013; Loizou, Tanner, Kumar & Kyriakopoulos, 2003; Yan, Jouandeau & Cherif, 2013).

Aerial refueling, also known as air-to-air refueling (AAR), is a critical aviation

capability that allows an aircraft to receive fuel mid-flight from another aircraft, thereby significantly extending its operational range, endurance, and mission flexibility (Huang, Zhou, Zheng, Xu, Zhang & Xiong, 2019). The fundamental logic behind aerial refueling lies in eliminating the need for aircraft to land for refueling, enabling sustained airborne operations, especially in remote or hostile environments where landing infrastructure may be unavailable or undesirable. This technique is particularly vital for long-range missions, reconnaissance, and rapid global deployment of air assets.

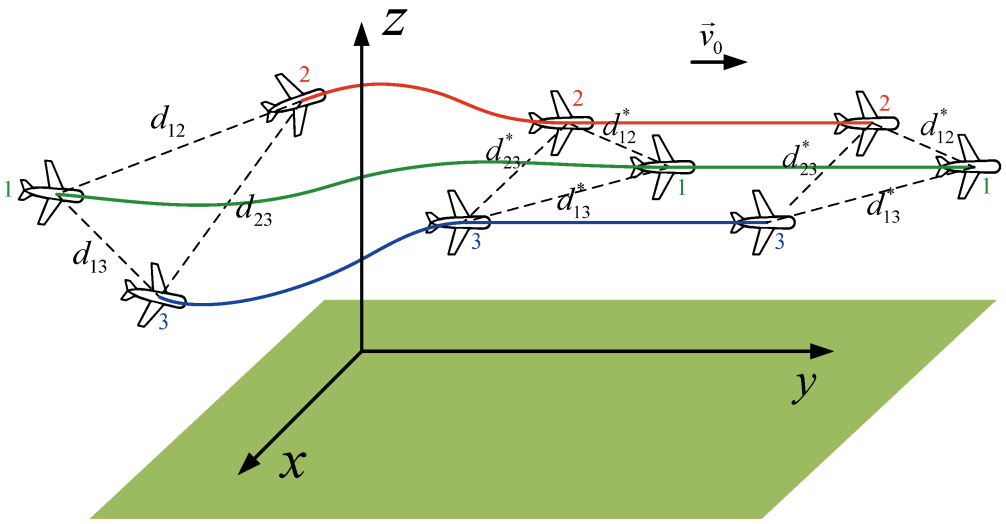

Figure 1.3 UAV formation control (Yan et al., 2022)

The origins of aerial refueling date back to the early 20th century, with the first successful attempts occurring in the 1920s using rudimentary hose-and-gravity methods. Over the decades, more advanced systems have been developed, including the probe-and-drogue -which is illustrated in Fig. 1.6- and flying boom methods, which remain in use today. These systems have been integrated into both manned and unmanned aircraft platforms, with military forces around the world.

Aerial refueling is utilized in a variety of strategic and tactical scenarios. In military operations, it supports fighter aircraft, bombers, reconnaissance platforms, and surveillance drones by allowing them to remain airborne longer, operate further from base, and respond more rapidly to emerging threats (Nalepka & Hinchman, 2005). In civilian contexts, aerial refueling is used in specialized missions such as firefighting and research flights. Its importance cannot be overstated—it acts as a force multiplier, enabling greater operational reach, sustained air presence, and logistical flexibility. As UAV technology advances, integrating aerial refueling capabilities into unmanned systems (Abeywickrama, Jayawickrama, He & Dutkiewicz, 2017) is a growing area of interest, promising even greater autonomy and mission endurance

Figure 1.4 Simultaneous aerial refueling with multiple receivers (Quantity & of russian Il-78 [Online image], air; for energy efficient inter-UAV collision avoidance, rus)

in future air operations.

While there has been considerable research focused on automating the aerial refueling process (LIN, HE & CHEN, 2024; REN & QUAN, 2024), both as receiver and tanker like in Fig. 1.5 but much of it has been limited to single-aircraft scenarios. But refueling multiple receivers simultaneously is an important increment to this technology, as shown in Fig. 1.4. As interest in multi-UAV systems continues to grow, a logical progression is the extension of autonomous aerial refueling capabilities to coordinated groups of UAVs (Lin, Morse & Anderson, 2003). Such an advancement would enable the benefits of aerial refueling—extended operational range, increased mission duration, and enhanced flexibility—to be fully realized within swarm-based operations. This thesis aims to integrate these concepts by developing an autonomous aerial refueling framework specifically designed for multi-UAV systems.

Figure 1.5 Aerial refueling with a tanker UAV (multi-agent rendezvous problem, mq2; to Air Refuelling – Key Force Multiplier [Online image], ref)

1.1. Problem Formulation

This section outlines the primary task that serves as the focal point of this thesis. While the baseline scenario is defined with specific characteristics, several variations will be explored throughout the manuscript to test system performance under different conditions.

The core task involves three UAVs acting as fuel receivers and a moving target representing the tanker aircraft. The coordinated refueling scenario is decomposed into the following sub-tasks:

• The receiver UAVs initiate an approach toward the tanker without maintaining a predefined formation.

• During the approach phase, the UAVs employ collision avoidance behaviors by adjusting their trajectories in response to the proximity of neighboring UAVs.

• If inter-vehicular distances fall below a critical threshold, the UAV farther from the tanker will reduce its speed to allow the closer UAV to proceed safely.

• Upon reaching a designated proximity to the tanker, the UAVs transition into a formation flight configuration, aligning at similar altitudes and preparing for the docking procedure.

The initial positions, attitudes, and airspeeds of all UAVs are assumed to be known and arbitrarily selected. Communication of position (Cui, Ge, How & Choo, 2009) and velocity data occurs among the UAVs and with the tanker; however, the specific communication protocol is beyond the scope of this study.

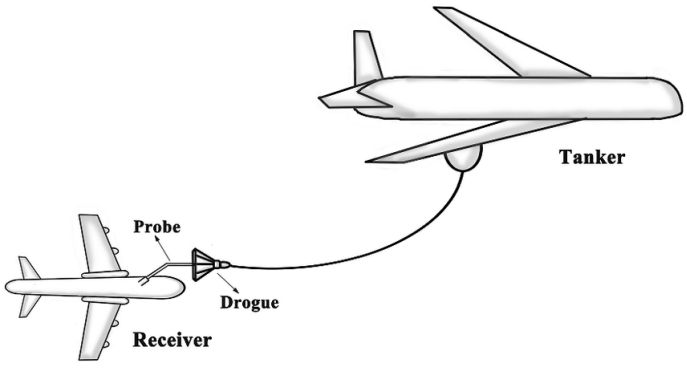

Figure 1.6 Illustration of docking for aerial refueling (Wu et al., 2021)

1.2. Thesis Contribution

The main contributions of this thesis are summarized as follows:

• Trajectory Generation Framework: A novel trajectory generation method is developed using virtual pulling and pushing forces. The approach leverages virtual spring-damper systems and charged-particle models to produce safe and efficient (Sheng, Yang, Tan & Xi, 2004) motion paths for UAVs.

• Controller Design: Position and attitude trajectory controllers are designed for non-holonomic Unmanned Ground Vehicles (UGVs) using a hierarchical control architecture based on virtual inputs. Additionally, waypoint-following PID controllers are implemented for UAV motion control.

• Collision Avoidance Algorithm: A new collision avoidance strategy inspired by real-world traffic dynamics is proposed, enabling coordinated motion among multiple agents with enhanced safety.

• Two-Phase Rendezvous Procedure: A two-stage approach is employed for the UAV-tanker rendezvous. During the initial approach phase, a relaxed trajectory generation strategy is utilized to minimize unnecessary constraints and allow flexible maneuvering. Upon reaching close proximity to the tanker, formation constraints are introduced to facilitate a structured and coordinated docking phase.

• Simulation Validation: The proposed methods are validated through simulation in both 2D and 3D environments. Test cases include groups of three UGVs approaching stationary and moving targets in 2D, as well as groups of three fixed wing UAVs in 3D.

1.3. Thesis Outline and Organization

The remainder of this thesis is structured as follows:

• Chapter 2 presents a literature review covering current research on autonomous aerial refueling, along with background information on the rendezvous problem. It provides a comprehensive overview of recent developments and established methodologies related to multi-agent gathering and coordination strategies.

• Chapter 3 focuses on high-level trajectory planning. Reference trajectories for the receiver UAVs are generated using virtual viscoelastic bonds, a method commonly employed in the robotics literature to ensure both safety and efficiency in path generation. We have also developed a novel collision avoidance strategy. When vehicles enter a predefined critical threshold, they dynamically adjust their velocities and trajectories to yield and avoid potential collisions, inspired by real-world traffic behavior.

• Chapter 4 addresses the motion control strategies required for trajectory tracking.

For two-dimensional (2D) scenarios involving Unmanned Ground Vehicles (UGVs), a cascaded control structure is implemented. For three-dimensional (3D) scenarios involving UAVs, a way-point-following PID-type controller is implemented.

• Chapter 5 presents the simulation results of the proposed framework. Various scenarios are tested in the simulation environment, including groups of differential-drive unmanned ground vehicles and fixed-wing UAVs. Special attention is given to collision scenarios, and the performance of the control strategies is evaluated through comparative plots of desired versus actual system states. Tracking errors are analyzed and insight about 3D visualization is provided. Scenario-specific analyses are conducted to interpret and contextualize the outcomes.

• Chapter 6 concludes the thesis by summarizing the key findings and suggesting potential directions for future research.

2. LITERATURE REVIEW

2.1. Autonomous Aerial Refueling (AAR)

Aerial refueling, also known as air-to-air refueling (AAR), is the process by which aircraft receive fuel mid-flight from a tanker aircraft. Traditionally, this process involves a high degree of human coordination between the tanker and receiver pilots. Two primary methods are employed: the probe-and-drogue system, and the flying boom system. Both demand precise manual control and communication, often under challenging conditions.

Autonomous Aerial Refueling (AAR) refers to the capability of unmanned aerial vehicles (UAVs) or piloted aircraft to engage in the refueling process without direct human intervention. This requires a combination of advanced sensing, navigation, control algorithms, and communication systems to execute the rendezvous, docking, and refueling phases autonomously.

The concept of autonomous aerial refueling began to gain traction in the early 2000s, aligned with the rise of UAVs for military applications. Early milestones include the DARPA Autonomous Airborne Refueling Demonstration (AARD) in 2006, which involved a modified F/A-18 engaging in semi-autonomous operations. Subsequent programs, such as the X-47B by Northrop Grumman and Boeing's MQ-25 Stingray, have pushed the boundaries of fully autonomous AAR systems.

The strategic advantage of AAR lies in extended mission endurance, improved operational flexibility, and reduced logistical footprints. For autonomous systems, the benefits are amplified, as they allow UAVs to operate in contested or remote environments without relying on ground control. AAR can also enable swarm-based operations and persistent surveillance by reducing the frequency of ground-based refueling stops.

Automating aerial refueling entails several complex challenges: precise relative navigation, dynamic trajectory planning, real-time communication, and fail-safe control systems. Technologies such as GPS-aided inertial navigation, vision-based sensing,

and machine learning are being integrated to facilitate the transition from human-supervised to fully autonomous AAR systems.

2.2. Multi-UAV Operations

Multi-UAV operations involve the coordinated deployment of multiple unmanned aerial vehicles to achieve a shared mission objective (Rao & Ghose, 2014; Ren & Beard, 2003). These systems can operate in cooperative, collaborative, or swarm configurations (Bishop, 2002; Monteiro & Bicho, 2002), depending on their communication architecture and autonomy level (Abeywickrama, Jayawickrama, He & Dutkiewicz, 2018).

The development of multi-UAV systems has evolved significantly over the past two decades. Initial research focused on military applications such as reconnaissance, target tracking, and area surveillance. More recently, civilian applications—including disaster response, agricultural monitoring, and logistics—have accelerated research in scalable and resilient multi-UAV frameworks.

The primary advantage of multi-UAV operations lies in distributed sensing and redundancy. A team of UAVs can cover more ground, reduce mission time, and increase fault tolerance compared to single-agent systems. Additionally, multi-UAV strategies enable task allocation, formation flying, and dynamic reconfiguration based on mission requirements.

Incorporating AAR into multi-UAV operations further enhances mission sustainability. Autonomous refueling allows UAV swarms to remain airborne for extended durations, conduct longer surveillance operations, or execute multi-phase missions without returning to base. This integration also necessitates advanced coordination and collision avoidance strategies (Jia & Li, 2007), particularly during the rendezvous and refueling phases.

2.3. The Rendezvous Problem

The rendezvous problem involves guiding one or more agents (e.g., UAVs) to meet at a designated location and time, often under motion constraints and in dynamic environments. In the context of AAR, the rendezvous problem focuses on synchronizing the approach of the receiver UAV with the tanker in both space and time. However, this problem also arises in other applications such as satellite docking, autonomous car platooning, and robotic swarm coordination (Dalamagkidis, Valavanis & Piegl, 2012).

2.3.1. Coordination Strategies

Centralized coordination

Centralized coordination involves a single control unit or agent responsible for computing and distributing trajectories to all UAVs. While this can yield globally optimal solutions, it suffers from scalability issues and vulnerability to single-point failures. In the context of AAR, centralized systems may use a command-and-control center to manage multiple receiver-tanker interactions.

Decentralized coordination

Decentralized strategies distribute control among all agents (Baras, Tan & Hovareshti, 2003), each making decisions based on local information and limited communication with peers (Borkowski, Gnatowski & Malec, 2001; Lalish, Morgansen & Tsukamaki, 2006). These approaches are more robust and scalable, making them suitable for dynamic, adversarial, or communication-limited environments. Decentralized coordination is particularly valuable when integrating AAR into large-scale UAV operations where centralized oversight is impractical.

2.3.2. Formation Control

Viscoelastic Bond Model:

Viscoelastic bond models treat UAVs as particles connected by virtual springs and dampers, enabling smooth and adaptive formation changes. These models are inspired by molecular dynamics and provide a physics-based framework for maintaining desired relative positions in a swarm or during rendezvous maneuvers.

Charged Particle Model:

In this model, UAVs are represented as charged particles that exert repulsive or attractive forces on each other based on distance. This technique can prevent collisions and maintain desired separation, especially in densely packed formations or during transition phases such as docking for refueling.

2.3.3. Collision Avoidance

Collision avoidance refers to the set of strategies and algorithms that prevent UAVs (Anderson, Fidan, Yu & Walle, 2008a) from colliding with each other, obstacles, or the environment. This is critical during close-proximity operations like formation flying and AAR.

In autonomous aerial operations, particularly with high-value assets and narrow

safety margins, collision avoidance is essential (Shao, Yan, Zhou & Zhu, 2019) for mission success and system integrity. The complexity increases with the number of vehicles, especially when operating in contested or cluttered airspace.

Common collision avoidance methods include:

- Reactive Approaches: Rely on local sensor data to execute immediate evasive maneuvers (e.g., optical flow or LiDAR-based methods).

- Predictive Approaches: Use trajectory forecasting and optimization to proactively avoid conflicts.

- Rule-Based Systems: Implement predefined rules such as "right-of-way" or minimum separation thresholds.

- Artificial Intelligence: Machine learning techniques, particularly reinforcement learning, are being explored to enable adaptive and experience-based avoidance strategies.

3. RENDEZVOUS PROBLEM AND PRE-DOCKING PHASE OF THE UAV SWARM

In this chapter, we present our proposed solution to the rendezvous problem for a UAV swarm approaching a tanker aircraft for aerial refueling. As outlined in Section 1.1, the problem involves multiple UAVs converging from arbitrary initial positions, attitudes, and airspeeds toward a moving tanker. The objective is to bring all UAVs within close proximity to the tanker, enabling subsequent autonomous refueling operations. The physical docking or interlocking process is beyond the scope of this work; our focus is limited to the safe and efficient approach phase. Two primary goals guide our solution: ensuring collision-free trajectories (safety) and achieving timely convergence (efficiency).

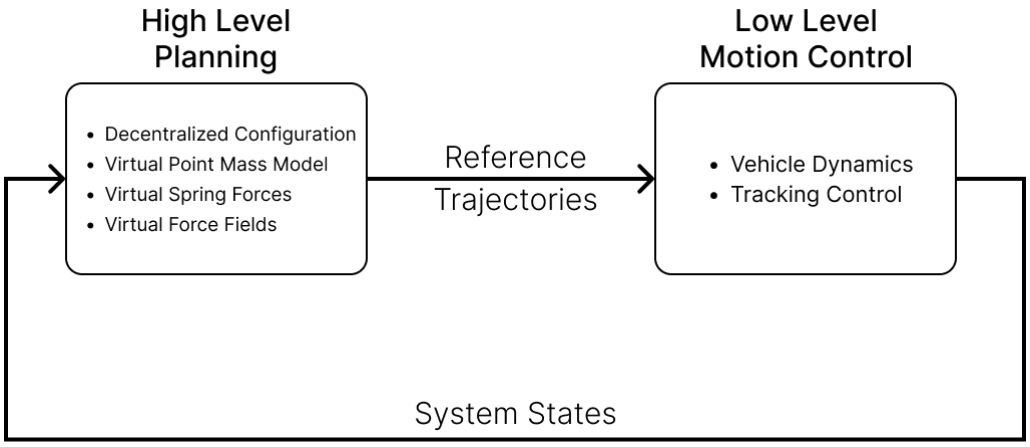

Figure 3.1 Hierarchical control structure

We frame this as a classical control problem, beginning with the generation of reference trajectories, followed by the implementation of motion control algorithms (Sun, Chen & Lv, 2022) to guide each UAV along its designated path in real time. The proposed framework is hierarchical and multi-layered, consisting of a high-level planning module and a low-level control layer. The structure can be seen in Fig. 3.1 The high-level planner itself operates in multiple interconnected stages. Initially, trajectories are generated using virtual spring and force field concepts (Hao, Lv,

Huang, Zhao & Chen, 2023). These trajectories are then passed to the vehicle control module. Real-time feedback from the UAVs is used to monitor progress, detect potential collisions, and trigger secondary planning phases. In the event of a collision threat, trajectories are dynamically adjusted, and reference paths are updated accordingly. This scheme can be seen in Fig. 3.2 All planning and control operations are performed online, with no reliance on precomputed or fixed path plans.

The rendezvous procedure is divided into two distinct stages. The first stage focuses on guiding the follower UAVs into close proximity with the tanker aircraft. The second stage, referred to as the pre-docking phase, ensures that each UAV reaches a suitable state and position for the subsequent interlocking operations to proceed smoothly. Specifically, each UAV must approach one of the three refueling probes on the tanker. To facilitate this, a dedicated secondary phase has been developed, which will be described in detail in Section 3.3.

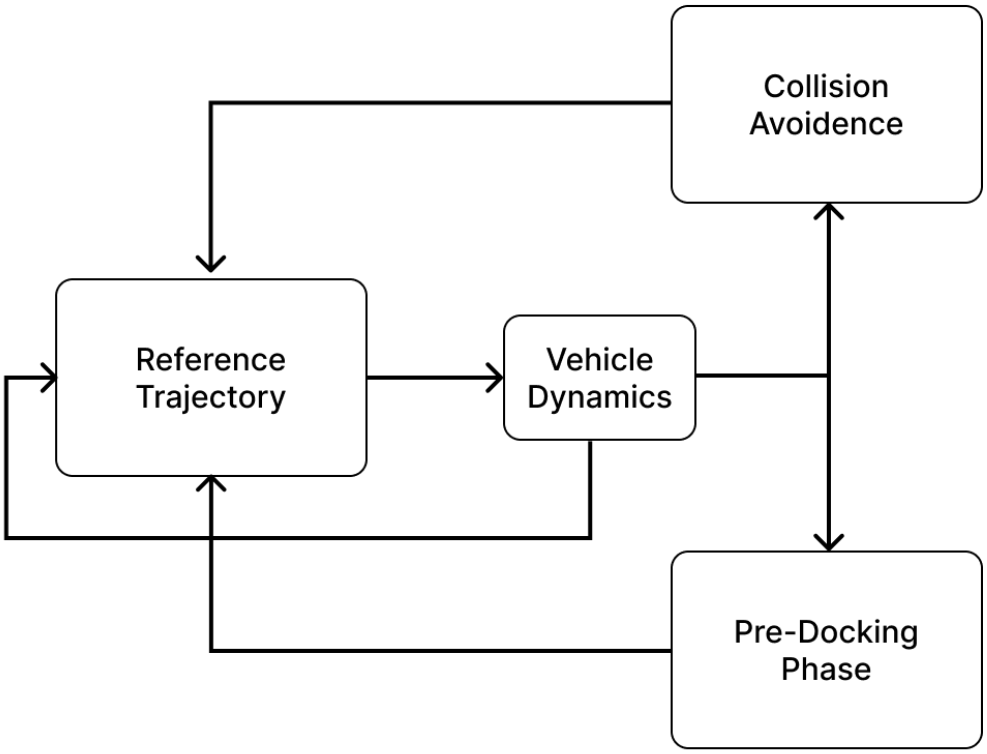

Figure 3.2 High level planner block diagram

3.1. Reference Trajectory Generation

3.1.1. Modeling UAVs as Particle Masses

The first step is the abstraction of vehicles as point mass particles and is shown in Fig. 3.3 This modeling approach simplifies the system by disregarding complex dynamics, such as non-holonomic constraints, and focuses instead on generating efficient and safe paths toward the target. The abstraction allows us to model vehicle motion as holonomic, enabling movement in any direction without the limitations imposed by physical vehicle orientation. The dynamics of each virtual particle are governed by

$$m\ddot{\mathbf{r}} + b\dot{\mathbf{r}} = \mathbf{F}_{\text{net}} \tag{3.1}$$

where $\mathbf{r} = [x, y, z]^T$ is the position vector of the virtual particle, m is the mass of the virtual particle, b is the viscous friction coefficient representing the resistive force from the environment, and F_{net} is the net force acting on the particle. This net force is the sum of attractive and repulsive forces exerted by the target and neighboring agents, respectively.

$$\mathbf{F}_{\text{net}} = \mathbf{F}_1 + \mathbf{F}_2 + \cdots + \mathbf{F}_n \tag{3.2}$$

While the orientation of the virtual particles is undefined in this model, most physical vehicle controllers require a reference heading. Thus, desired orientation will be derived from the velocity vector of each virtual mass.

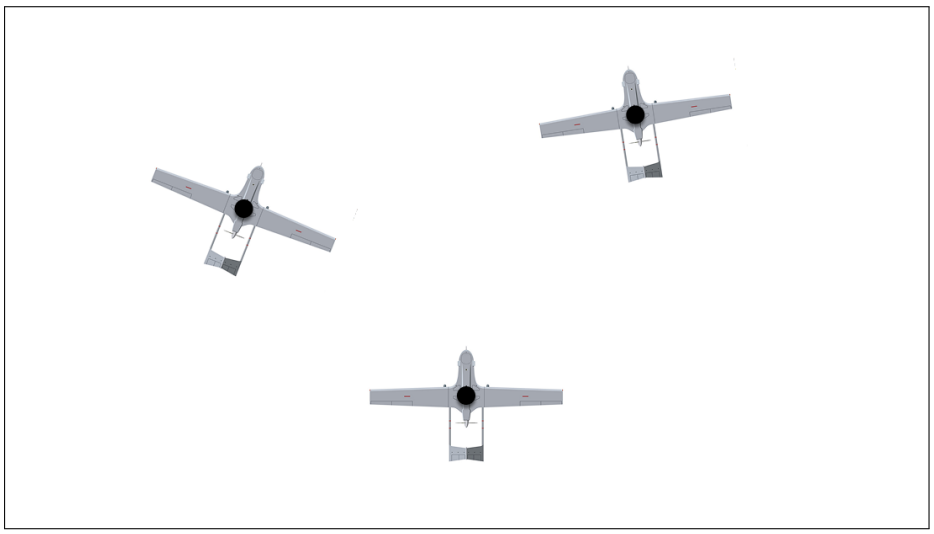

Figure 3.3 Abstraction of UAVs as particle masses

3.1.2. Virtual Spring Model

To drive each vehicle toward the rendezvous target, virtual attractive forces are modeled using nonlinear spring dynamics. Fig. 3.4 shows an illustration of the virtual spring bonds. Given that the rendezvous strategy is decentralized, each vehicle computes its own trajectory based on locally sensed or communicated information. This autonomy ensures scalability and robustness. The virtual linear spring force acting on a vehicle is given by

$$\mathbf{F}_{\text{spring}} = -k\mathbf{d} \tag{3.3}$$

where k is the spring coefficient, and $\mathbf{d}$ is the distance vector, measured from the target to the vehicle.

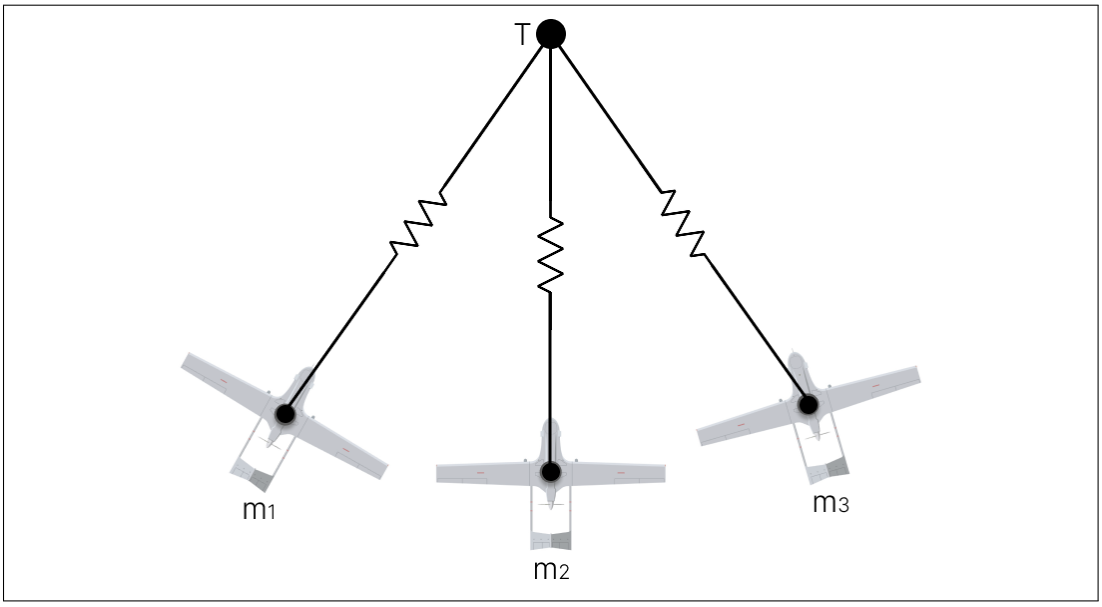

Figure 3.4 Virtual spring forces between UAVs and the target

While a linear spring force is straightforward to implement, it presents several limitations. Primarily, because the spring force is directly proportional to the distance between the UAV and the target, large initial separations can result in excessive pulling forces. This leads to unrealistically high desired speeds for the UAVs. Since the UAVs typically start at significant distances from the tanker, the resulting acceleration demands become problematic. These high acceleration requirements can strain the hardware, result in inefficient movement, cause abrupt velocity changes, degrade trajectory tracking through overshoot, and compromise safety due to aggressive, full-throttle maneuvers. To address these challenges, we introduce a nonlinear modification to the spring coefficient. Specifically, we designed a force profile that

remains relatively gentle at larger distances but becomes increasingly stiff as the UAVs approach the tanker. To achieve this behavior, we developed a sigmoid-based spring coefficient, denoted as k_s:

$$k_s = \frac{k}{\alpha}\left(1 + \frac{\alpha}{1 + e^{|d|}}\right) \tag{3.4}$$

where $|d|$ is the distance between the vehicle and the target, α is a parameter which controls the scaling of the spring coefficient, and k is the base spring constant.

Unlike linear springs, which produce excessively strong forces at large distances and diminish rapidly upon convergence, this nonlinear spring is designed for a smoother convergence. In particular, a sigmoid function is incorporated into the spring coefficient, resulting in relaxed forces at longer distances and increasing stiffness as the vehicle nears the target and the plot of it can be seen in Fig. 3.5. This behavior improves overall formation control and prevents abrupt maneuvers near convergence.

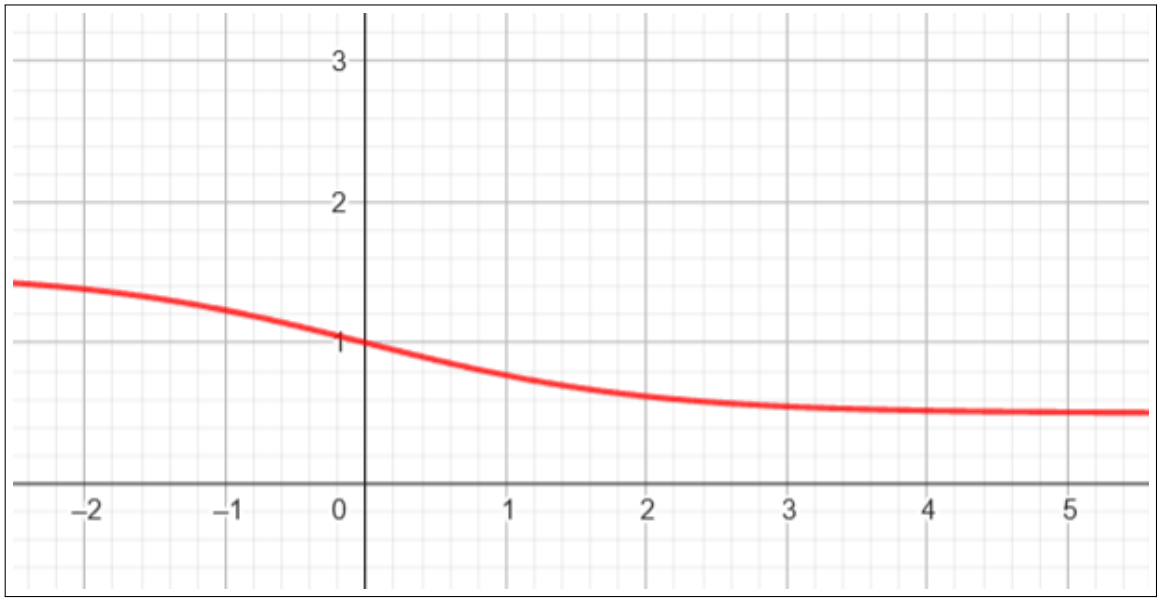

Figure 3.5 Sigmoid function developed for the non-linear spring coefficient

At greater distances, the virtual spring exerts a weaker, gentler pulling force on the vehicle due to its lower stiffness. As the distance decreases, the spring becomes stiffer, gradually approaching its original pulling coefficient. When combined with the non-linear coefficient, the resulting virtual spring force is expressed as:

$$\mathbf{F}_{\text{spring}} = -k_s \mathbf{d} \tag{3.5}$$

3.1.3. Charged Particle Model

While spring forces attract all agents toward a common goal, they may also cause the vehicles to cluster too closely (Zhang, Yan & Zhang, 2018), increasing the risk of collision. To address this, repulsive forces seen in Fig. 3.6 are introduced between vehicles (Pan, Zhang, Xia, Xiong & Shao, 2022), inspired by the physics of same-charged particles. These repelling forces are inversely proportional to the inter-vehicle distance and are deactivated once a predefined safety threshold is exceeded. This design simplifies computation, reduces unnecessary interactions among distant vehicles, and allows more efficient path generation without over-dispersing the swarm.

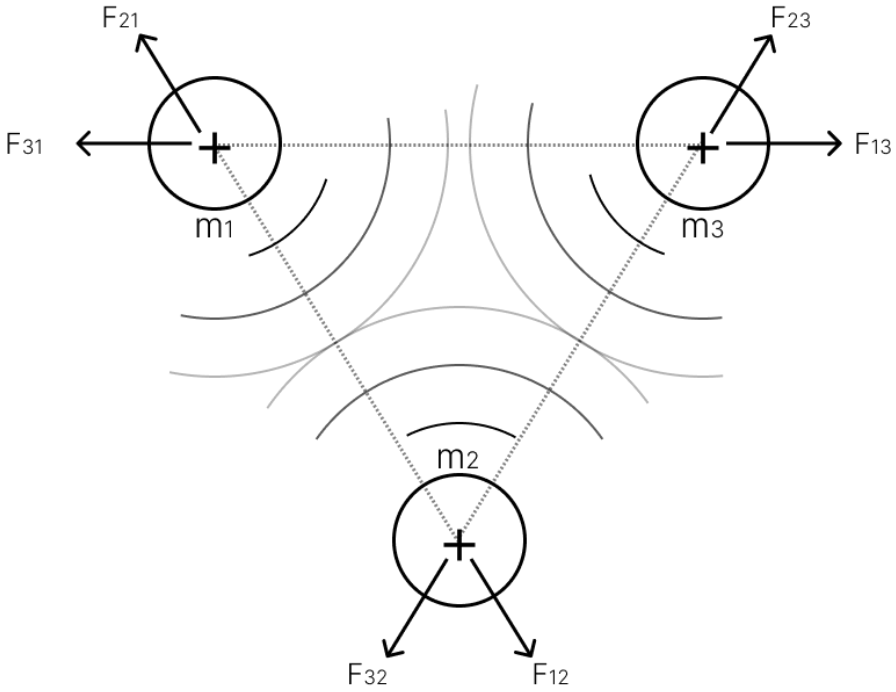

Figure 3.6 Charged particles repelling each other

The quadratic nature of these forces ensures that as vehicles approach dangerously close proximity, the repulsion becomes strong enough to enforce safe separation (Paul, Krogstad & Gravdahl, 2008). The synergy between the pulling and pushing forces forms the foundation of the proposed trajectory generation framework.

The repulsion force exerted by the i-th vehicle to the j-th vehicle is:

$$\mathbf{F}_{\text{rep, ij}} = \begin{cases} \frac{k_r}{|d|^2}\hat{u}_{ij}, & \text{if } |d| < d_{\text{critical}} \\ 0, & \text{otherwise} \end{cases} \tag{3.6}$$

where k_r is the repulsion force coefficient, $\hat{u}_{ij}$ is the unit vector from i-th vehicle

to j-th vehicle, $|d|$ is the distance between these vehicles and $d_{critical}$ is the pre-defined critical distance after which, no more repulsion force will be exerted. The combination of virtual forces are illustrated in Fig. 3.7

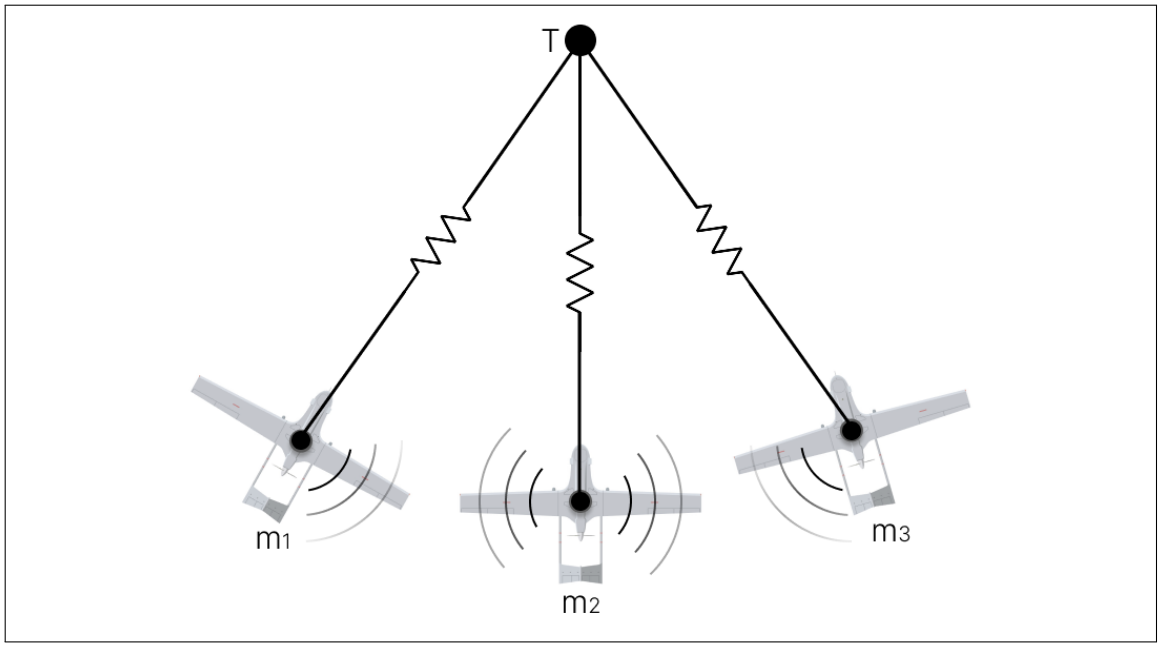

Figure 3.7 Combination of virtual attractive and repulsive forces

3.1.4. 2D Framework and Extension to 3D Cases

Both the force fields and virtual spring forces are decoupled along separate axes, allowing the force components to be independently analyzed and applied in the x, y, and z directions.

Initial development and validation of the proposed approach were carried out in a 2D ground vehicle (UGV) context to simplify the analysis and serve as a proof of concept. The method is subsequently extended to three-dimensional space for application to UAVs.

This extension involves augmenting the dynamic and positional equations with a third dimension (z-axis). The principles of virtual forces, trajectory generation, and motion control remain unchanged; only the spatial representation and force vectors are adapted to accommodate full 3D motion.

Spring forces acting along x, y and z axes are defined as

$$\mathbf{F}_{\text{spring},x} = -k_s \cdot \Delta x \hat{i} \tag{3.7}$$

$$\mathbf{F}_{\text{spring},y} = -k_s \cdot \Delta y \hat{j} \tag{3.8}$$

$$\mathbf{F}_{\text{spring},z} = -k_s \cdot \Delta z \hat{i} \tag{3.9}$$

where Δx, Δy and Δz are the distances between the target and vehicles along the x, y and z axes, respectively. Each of them are measured by subtracting the coordinates of the target from the i-th vehicle.

Virtual electric charge forces acting along each axes are defined as

$$\mathbf{F}_{\text{repulsion},x} = \frac{k_r}{(\Delta x)^2} \hat{i} \tag{3.10}$$

$$\mathbf{F}_{\text{repulsion},y} = \frac{k_r}{(\Delta y)^2} \hat{j} \tag{3.11}$$

$$\mathbf{F}_{\text{repulsion},z} = \frac{k_r}{(\Delta z)^2} \hat{k} \tag{3.12}$$

Virtual pushing and pulling forces form the foundation of the reference trajectory generation process (Budiyanto, Cahyadi, Adji & Wahyunggoro, 2015). Following this initial stage, additional layers—namely collision avoidance and the second-phase transition—are applied. The outputs from these layers dynamically influence and modify the reference trajectories to ensure continued safety and effectiveness (bo Chen, chen Luo, song Mei, qiao Yu & long Su and, 2016). The following sections will provide a detailed explanation of the collision avoidance algorithm and the mechanism governing the transition to the docking phase.

3.2. Collision Avoidance

Although repulsive inter-agent forces contribute to safer trajectories, they do not guarantee complete collision avoidance. There are two primary concerns: (1) the net forces may still generate paths that intersect under certain initial conditions, and (2) tracking errors in the controllers may cause real vehicles to deviate from the reference trajectories. To address these challenges, a dedicated collision avoidance mechanism is implemented as a supplementary layer (bo Chen et al., 2016). This algorithm operates independently of the trajectory generation process and ensures that real-time deviations do not result in collisions.

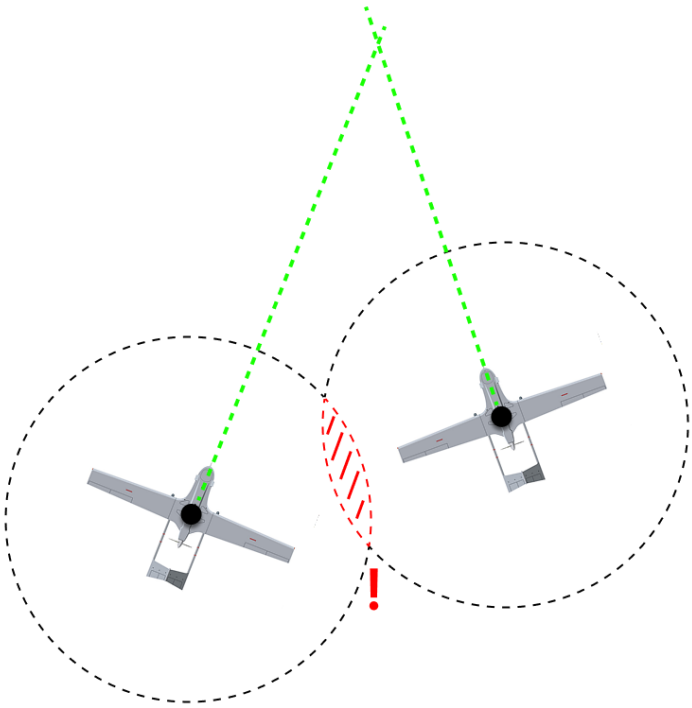

Figure 3.8 Collision detection

Collision avoidance is a well-studied topic in the field of robotics, and numerous approaches have been developed to address it. Generally, a collision avoidance system consists of two primary components:

1. *Collision Detection*

2. *Collision Response*

For any effective avoidance mechanism, agents must first be able to detect potential collisions. A wide variety of sensors and techniques are employed for this purpose in robotics, including image-based methods, ultrasonic sensors, LiDAR, GPS, and others. These technologies provide different ways of identifying when two agents are at risk of a dangerous proximity.

In our approach, we assume the existence of an established communication network that enables UAVs to share position and velocity information in real time. Based on this shared data, each UAV independently computes its distance to all other agents on board, using this information to assess the risk of collision. When the distance between any two UAVs falls below a predefined safety threshold, collision detection flags are triggered, as shown in Fig. 3.8.

Once a potential collision is detected, the system must generate an appropriate response. Traditional approaches often rely on abrupt maneuvers, such as

sharp turns or rapid speed changes, to avoid impending collisions. However, for UAVs—operating at high speeds and subject to aerodynamic constraints—such maneuvers can be energetically inefficient and potentially destabilizing, leading to reduced performance or even stalling.

To address these challenges, we propose a novel, more graceful collision response mechanism inspired by real-world driving etiquette. Upon detection of a potential collision, both UAVs involved trigger their collision flags. The UAV that is farther from the tanker yields by slowing down, allowing the other vehicle to proceed. This behavior is achieved by relaxing the spring coefficient used in the trajectory generation of the trailing UAV, resulting in a lower desired speed. Additionally, the repulsion coefficients for both vehicles are increased, encouraging them to diverge more strongly and avoid further proximity. This process is presented in a flowchart in Fig. 3.9

This approach yields a smooth and energy-efficient collision avoidance behavior, balancing safety with aerodynamic and control constraints, and ensuring continuous progress toward the rendezvous objective.

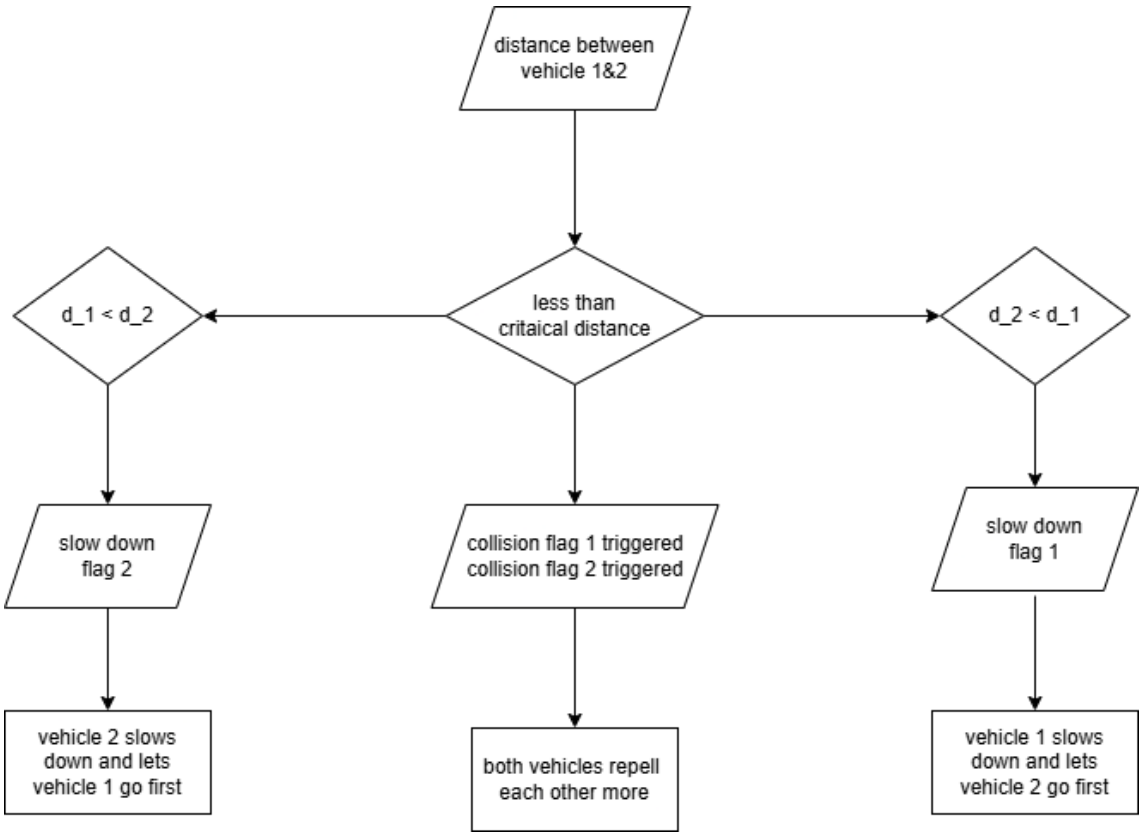

Figure 3.9 Rule-based decision making of the collision avoidance algorithm

Once the slowdown warning is triggered, the spring coefficient of the corresponding vehicle is reduced by a predetermined percentage. This reduction decreases the magnitude of the virtual pulling force, which in turn lowers the reference speed generated by the trajectory planner. As a result, the farther UAV slows down, while the closer one continues unaffected. The updated virtual spring force is given by:

$$\mathbf{F}_{\text{spring, slow}} = c_{\text{slow}} \cdot k_s \cdot \mathbf{d}, \quad \text{where } 0 < c_{\text{slow}} < 1 \tag{3.13}$$

In addition to the slowdown mechanism, repulsive forces are also increased between UAVs identified as being in potential collision danger. The underlying logic is similar: when a collision warning is triggered, the repulsive force between the involved vehicles is amplified using a scaling coefficient. This enhancement adds a "shoving" effect on top of the slowdown, further reducing the likelihood of a collision.

For example, if a potential collision is detected between UAV-i and UAV-j, the updated repulsion force exerted on UAV-j is given by

$$\mathbf{F}_{\text{repulsion, increased}} = c_{\text{rep}} \cdot \frac{k_r}{|d|^2} \hat{u}_{ij}, \quad \text{where } c_{\text{rep}} > 1 \tag{3.14}$$

where $\hat{u}_{ij}$ is the unit vector directed from the i-th vehicle to the j-th vehicle.

The selection of the repulsion and slowdown coefficients is a critical part of the system's tuning process. To ensure both safety and efficiency in collision avoidance, several key parameters must be carefully defined. The relationship between these parameters is primarily influenced by the cruise speeds of the UAVs, which determine how quickly the system must respond to potential collisions. This response is governed by factors such as the safe radius of each vehicle, the slowdown coefficient, and to a lesser extent, the repulsion scaling coefficient.

As UAV speed increases, the collision warning radius must also be expanded to allow sufficient time for avoidance maneuvers. The degree to which the trailing UAV slows down is equally important: it must decelerate enough to avoid entering the projected path of another vehicle, but not so much that it drops below its minimum cruising speed, risking a stall. Therefore, this tuning process must be performed with careful consideration to balance responsiveness and vehicle stability.

3.3. Pre-Docking Phase

Aerial refueling is a well-established procedure, with standardized protocols developed over decades of use. Most conventional tanker aircraft are equipped with three

refueling probes—two located at the wingtips and one at the rear of the fuselage. This capability has served as a key design consideration in enabling simultaneous refueling of multiple UAVs, offering an alternative to purely sequential refueling operations.

An aerial refueling mission typically consists of four main phases: rendezvous, docking, refueling, and separation. This thesis focuses on the rendezvous and pre-docking stages. During these phases, the objective is to guide multiple UAVs from dispersed starting positions into close proximity with the tanker, followed by preparation for docking through structured formation flight. While formation flight could be imposed from the beginning, doing so would introduce unnecessary constraints early in the maneuver. Given the UAVs' initially diverse and distant positions, forcing a rigid formation prematurely would be both inefficient and impractical.

To address this, we propose a two-stage approach. In the first stage, the UAVs converge toward the tanker without any formation constraints. The primary objectives are to avoid collisions and to reduce the separation between each UAV and the tanker. Trajectory generation in this phase is based on virtual spring and charged particle models. UAV states are continuously evaluated by a collision avoidance layer, which enforces safety through real-time updates. Importantly, no attractive forces are applied between UAVs; instead, only repulsive forces are used to prevent close encounters. This ensures safe navigation but can result in an unstructured clustering of UAVs near the tanker, which is unsuitable for initiating the docking phase.

This leads to the second stage, referred to as the pre-docking phase. In Fig. 3.10 the flowchart of the 2nd phase transition is shown. Once all UAVs have reached a sufficiently close distance to the tanker and maintain safe separation among themselves, the system recognizes that the rendezvous phase is complete. At this point, a more structured formation becomes necessary. A triggering mechanism initiates the pre-docking phase, during which an ordering algorithm calculates the azimuth angles between each UAV and the tanker. Based on these angles, UAVs are assigned to one of three roles: left, center, or right. These assignments correspond to the physical locations of the tanker's three refueling probes.

Following this assignment, the reference attraction points for each UAV are updated from the tanker's center of mass to the specific probe locations. Consequently, UAVs no longer cluster toward the central axis but instead maneuver toward their assigned docking positions: left and right UAVs move toward the wingtips, while the center UAV aligns with the rear fuselage. This transition resolves the clustering issue and ensures a smooth and coordinated approach to the refueling positions.

In the final configuration, each UAV maintains a constant velocity and stable position in close proximity to its designated probe, creating the conditions necessary for the individual interlocking procedures to be initiated. This concludes the multi-agent rendezvous strategy proposed in this thesis.

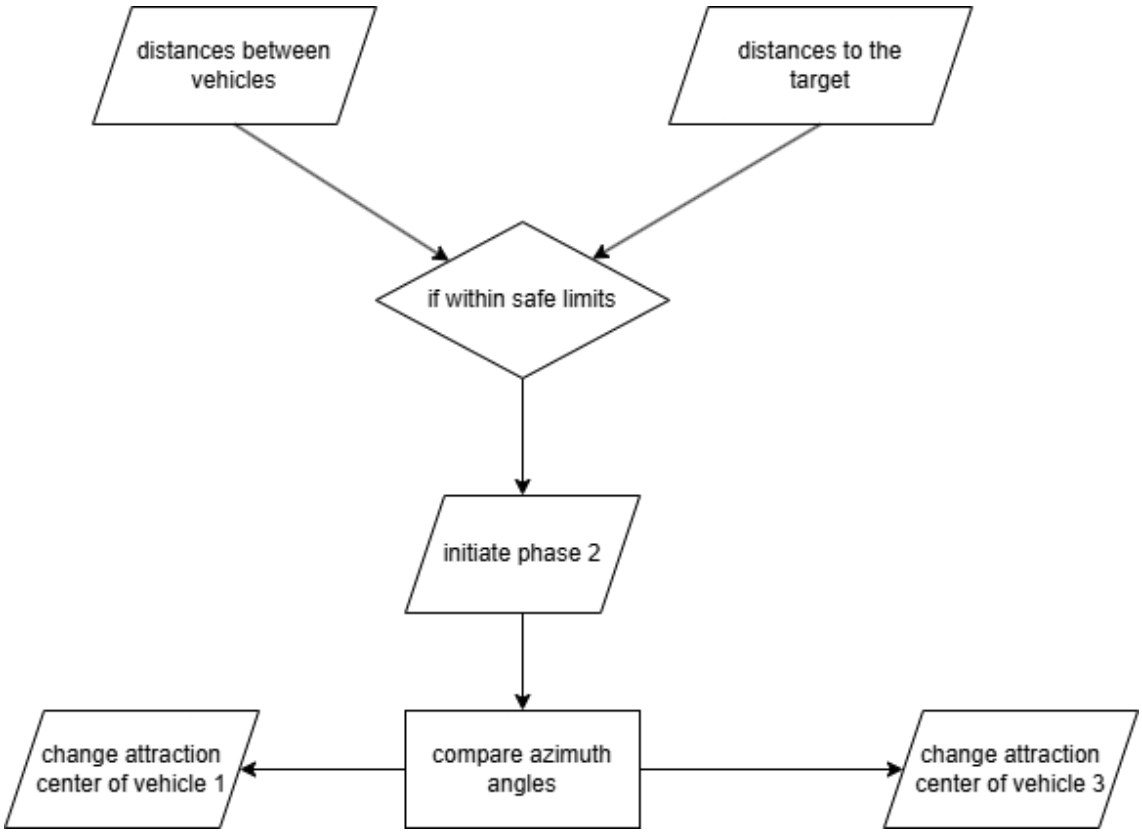

Figure 3.10 Changing attraction centers for the pre-docking phase

The initial step in the phase transition from rendezvous to pre-docking involves calculating the azimuth angles between each vehicle and the target. These angles are defined as:

$$\theta_i = atan2(\Delta y_i, \Delta x_i) \tag{3.15}$$

In this equation, θ_i represents the azimuth angle of the i-th UAV, Δy_i is the y-axis distance between the vehicle and the target, and Δx_i is the x-axis distance. The z-component of the distance is not considered, as vehicle assignments to the probes are based on their positions in the x-y plane. After calculating the azimuth angles for all vehicles, we sort them in descending order. This sorting process provides the relative positions of the vehicles from right to center to left, with respect to the target and is shown in Fig. 3.11

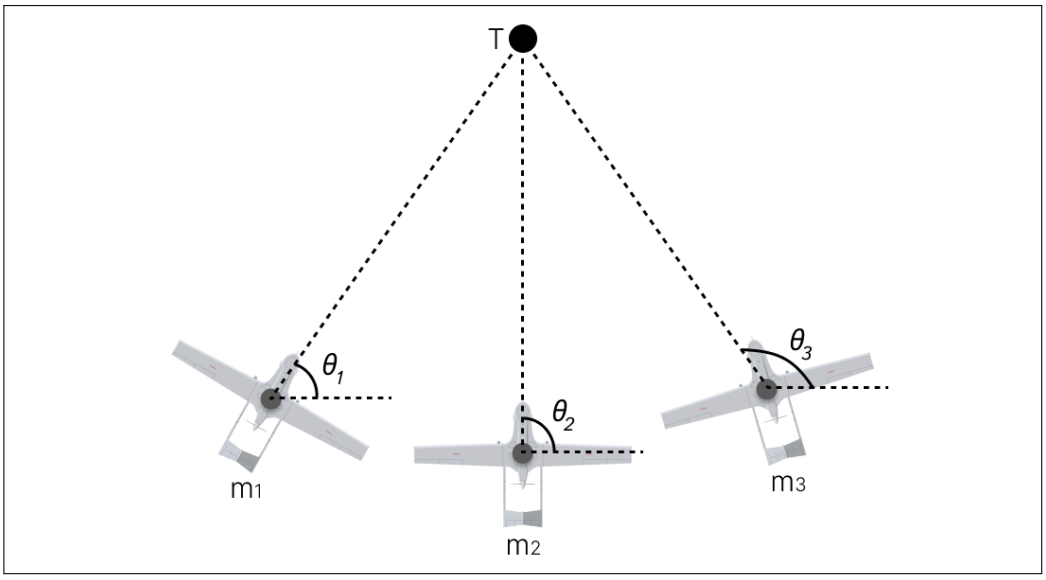

Figure 3.11 Ordering of UAVs according to the azimuth angles

Once the vehicles have been sorted, we assign numbers to the UAVs from left to right: 1, 2, and 3. UAV 2 is attracted to the same center as before and aims to reach the rear of the fuselage. Meanwhile, UAV 1 is directed to the right wing, and UAV 3 to the left wing. To facilitate this, we shift the attraction centers for UAVs 1 and 3 a few meters to the right and left of the tanker's center, respectively. In addition to adjusting the attraction centers, we also increase the virtual spring coefficients. This adjustment helps reduce the distance between the tanker and the UAVs. By sorting the vehicles and directing them to distinct positions, the potential for clustering or collision is minimized, allowing us to relax the safety parameters slightly in order to form a more efficient docking configuration.

To achieve this, we first compute a vector that is orthogonal to the direction of motion of the tanker, aligning it with the wing axis. Since both the fuselage and wings lie in a two-dimensional plane, the calculations can be performed using 2D vectors. Given the velocity vector of the tanker:

$$\vec{v} = \begin{bmatrix} a \\ b \end{bmatrix} \tag{3.16}$$

The unit vector along the wingspan, which is orthogonal to $\vec{v}$, is given by:

$$\vec{n} = \frac{1}{\sqrt{a^2 + b^2}} \begin{bmatrix} b \\ -a \end{bmatrix} \tag{3.17}$$

Using this, the centers of attraction for UAVs 1 and 3 are defined as:

$$\vec{P}_{\text{attraction,1\&3}} = \vec{C}_{\text{attr}} \pm \beta\vec{n} \tag{3.18}$$

where C_{attr} is the position vector of the initial center of attraction —toward which UAV 2 will continue to be drawn—and β represents the distance of the new attraction centers from the center of the fuselage.

$$\mathbf{F}_{\text{spring,dock}} = c_{\text{dock}} \cdot k_s \cdot \mathbf{d} \quad \text{where} \quad c_{\text{dock}>1} \tag{3.19}$$

In addition to adjusting the attraction centers, we also increase the virtual spring coefficients. This adjustment helps reduce the distance between the tanker and the UAVs. By sorting the vehicles and directing them to distinct positions, the potential for clustering or collision is minimized, allowing us to relax the safety parameters slightly in order to form a more efficient docking configuration.

Up to this point, our focus has been on the high-level planning aspect of the problem, with particular emphasis on reference trajectory generation. In this chapter, we introduced the attractive and repulsive force models and provided a detailed explanation of their mechanisms. In Chapter 4, we shift our attention to the trajectory tracking problem. This next stage begins with modeling the relevant vehicles, followed by the development of local control strategies that enable individual agents to follow the generated reference trajectories. To establish a solid foundation, we will first validate our approach in two-dimensional proof-of-concept scenarios using unmanned ground vehicles (UGVs), before extending the framework to three-dimensional environments involving fixed-wing unmanned aerial vehicles (UAVs).

4. VEHICLE MODELING AND DISTRIBUTED MOTION CONTROL FOR UGVS AND UAVS

To achieve coordinated rendezvous, the generated reference trajectories must be accurately tracked by the vehicles. An example of this is shown in Fig. 4.1. This presents a challenge, as the vehicles are non-holonomic, yet the trajectories do not account for these constraints. Additionally, managing a multi-vehicle system introduces complexities such as path optimization and collision avoidance. To simplify the problem, most coordination issues are addressed at a higher-level planning layer, incorporating repulsive forces between vehicles. As a result, the focus shifts to solving individual tracking problems for each vehicle. This reduces the overall task to a more straightforward local reference tracking problem, which we address by synthesizing dedicated controllers for each vehicle in the group.

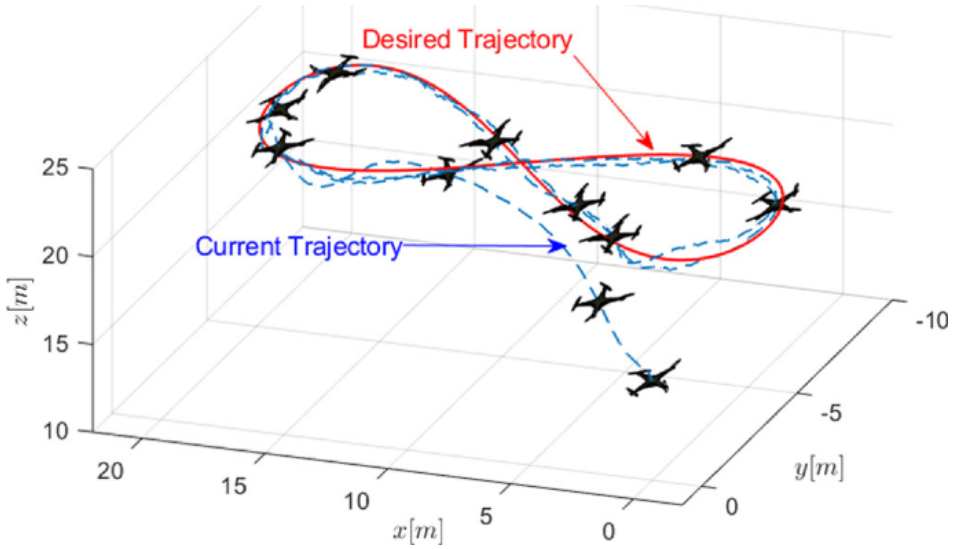

Figure 4.1 Reference trajectory tracking (Anderson et al., 2008b)

We begin by simplifying the scenario to a 2D case, which serves as a testbed for the eventual 3D implementation. In the 2D rendezvous setup, we utilize non-holonomic differential drive unmanned ground vehicles (UGVs). Once the desired coordination performance is achieved in these proof-of-concept scenarios, we progress to more

realistic aerial refueling cases, including scenarios with dynamic targets using fixed-wing UAVs. For the test simulations, we classify the scenarios into three categories: 2D with a stationary target, 2D with a moving target and 3D with a moving target.

4.1. Controller Development for UGVs

To establish a proof-of-concept testbed, we begin by applying the previously discussed trajectory generation techniques to 2D scenarios. For this purpose, we use differential drive unmanned ground vehicles (UGVs). The planner-generated trajectories must be tracked by the physical robots to accomplish coordinated tasks. This tracking is non-trivial because the planned trajectories are holonomic (Vlantis, Vrohidis, Bechlioulis & Kyriakopoulos, 2018), while most real-world robotic platforms are non-holonomic.

Moreover, the generation of dynamically feasible trajectories was not emphasized in the initial planning phase. Therefore, an appropriate controller synthesis is essential to ensure compatibility with different kinematic and dynamic models.

This chapter focuses on the modeling and control of two types of robots used as validation platforms in this thesis: non-holonomic mobile robots (van den Broek, van de Wouw & Nijmeijer, 2009) and fixed-wing-type unmanned aerial vehicles (UAVs). Non-holonomic robots are among the most commonly used platforms in multi-robot system (MRS) coordination tasks due to their affordability and wide availability. The non-holonomic constraint imposes restrictions on the direction of motion, which complicates the mathematical representation of the system and, consequently, the controller design.

The control of non-holonomic systems, particularly unicycle-type mobile robots, has been extensively studied in the literature (Spletzer, Das, Fierro, Taylor, Kumar & Ostrowski, 2001; van den Broek et al., 2009). In this section, we review the unicycle model and develop a hierarchical control scheme using virtual control inputs to enable trajectory tracking.

4.1.1. Kinematic Model for UGVs

The standard kinematic model for a unicycle-type robot can be described using its linear and angular velocities. The equations of motion are:

$$\dot{x} = u_1 \cos\theta, \tag{4.1}$$

$$\dot{y} = u_1 \sin\theta, \tag{4.2}$$

$$\dot{\theta} = u_2, \tag{4.3}$$

In Fig. 4.2, x and y represent the Cartesian coordinates of the robot's center of gravity in the earth-fixed frame, and θ denotes its orientation angle with respect to the horizontal axis.

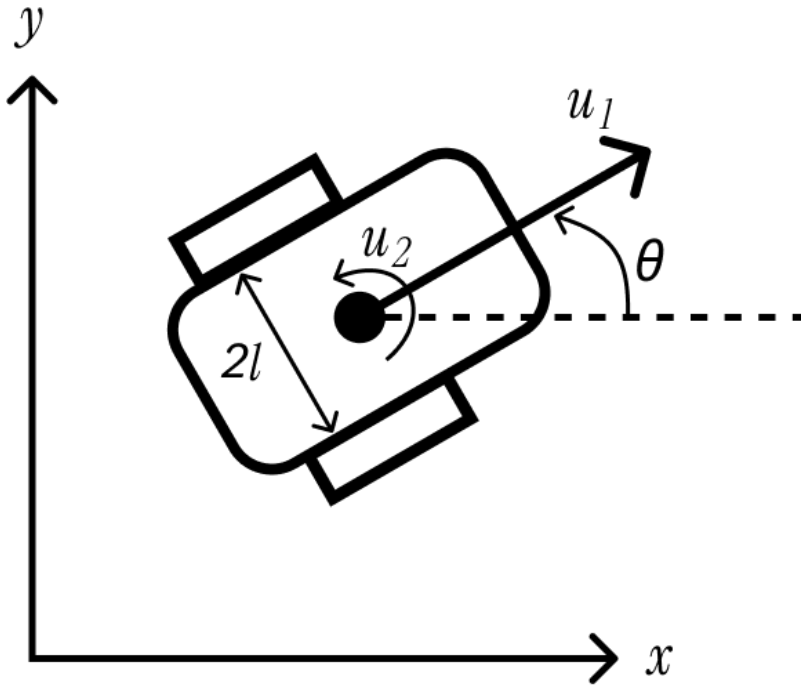

Figure 4.2 Control inputs for the differential drive UGV

The control inputs u_1 and u_2 correspond to the robot's linear and angular velocities, respectively, which are used to control its motion. A schematic of the unicycle-type UGV is shown in Fig. 4.4. The inputs u_1 and u_2 are directly related to the angular velocities of the robot's right and left wheels, denoted by u_R and u_L. This relationship is defined by

$$u_1 = \frac{1}{2}(u_R + u_L),$$
$$u_2 = \frac{1}{2l}(u_R - u_L),$$

where l is half the distance between the two wheels.

After deriving the kinematic model for the UGVs, we proceed directly to the control design without incorporating dynamic modeling. This approach is justified because, under the non-holonomic no-slip condition, the system's dynamics are constrained to follow the kinematics.

4.1.2. UGV Controller Design

As seen from the kinematic equations, the model has two control inputs—u_1 (linear velocity) and u_2 (angular velocity)—which are used to control three output states that define the robot's pose: $[x, y, \theta]^T$. In control theory, such a system is referred to as *underactuated*, meaning it has fewer control inputs than state variables. Controlling underactuated systems is notably more challenging due to these inherent limitations.

To enable the non-holonomic UGV to follow a desired trajectory $[x_d(t), y_d(t)]$, a hierarchical (or cascaded) control scheme is employed. In this approach, an *outer loop* regulates the position states and computes a desired orientation angle, which is then passed to an *inner loop* responsible for controlling the robot's heading. This structure is illustrated in Fig. 4.2.

The control design decomposes the trajectory tracking problem into two subproblems:

- **Outer Loop:** Assume holonomic behavior to determine the trajectory-tracking control law, temporarily ignoring non-holonomic constraints.
- **Inner Loop:** Given the system's non-holonomic nature, compute the required heading angle and ensure the robot's orientation aligns with this reference.

This cascaded structure shown in Fig. 4.3 allows the robot to approximate holonomic behavior while respecting its kinematic constraints.

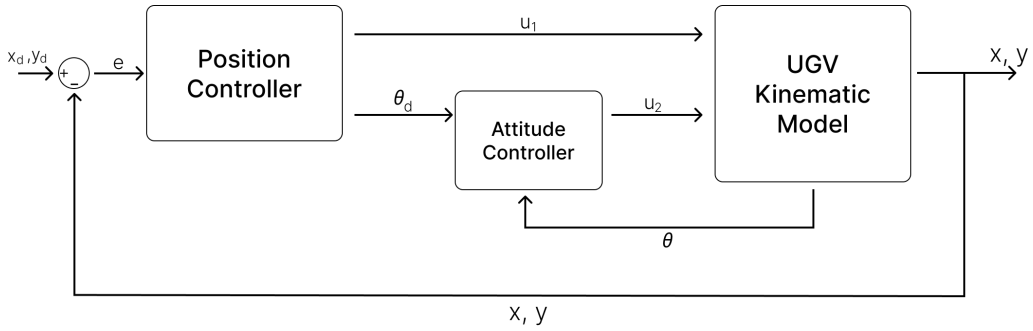

Figure 4.3 Cascaded controller structure for differential drive UGV

Position Control

The position controller is responsible for generating the desired orientation (θ_d) to be tracked by the attitude controller, while ensuring that the UGV follows a feasible trajectory. This controller is derived using the first two equations of the kinematic model (Eq. 4.2), which describe the motion in the x and y directions.

The control design follows a virtual control input approach, where artificial control signals are introduced to simplify the trajectory tracking problem. The objective is to drive the position errors—the difference between the actual and desired positions—to zero. This is achieved through a cascaded control structure, typically employing PID controllers.

We begin by defining the position errors as:

$$e_x = x_d - x,$$
$$e_y = y_d - y,$$

where x_d and y_d are the desired position coordinates. By differentiating these errors with respect to time, we obtain the error dynamics, which will form the basis for designing the virtual control laws.

$$\dot{e}_x = \dot{x}_d - \dot{x},$$
$$\dot{e}_y = \dot{y}_d - \dot{y}.$$

For a feasible, non-holonomic trajectory, we define the virtual control inputs μ_x and μ_y as the derivatives of the position states x and y, respectively:

$$\mu_x = \dot{x}, \quad \mu_y = \dot{y}.$$

Substituting these into the error dynamics yields:

$$\dot{e}_x = \dot{x}_d - \mu_x, \quad \dot{e}_y = \dot{y}_d - \mu_y$$

Since the system is first-order, a Proportional-Integral (PI) controller is sufficient to eliminate the steady-state error. To avoid dependence on the derivatives of the desired x and y values, feedforward terms are incorporated alongside the PI control components in the virtual control inputs:

$$\dot{e}_x = \dot{x}_d - \left(\dot{x}_d + K_{p,x}e_x + K_{i,x}\int e_x\,dt\right)$$
$$\dot{e}_y = \dot{y}_d - \left(\dot{y}_d + K_{p,y}e_y + K_{i,y}\int e_y\,dt\right)$$

To implement this approach, the virtual control inputs are chosen as follows:

$$\mu_x = \dot{x}_d + K_{p,x}e_x + K_{i,x}\int e_x\ dt,$$
$$\mu_y = \dot{y}_d + K_{p,y}e_y + K_{i,y}\int e_y\ dt.$$

With these virtual inputs, the error dynamics become:

$$\dot{e}_x = -K_{p,x}e_x - K_{i,x}\int e_x\,dt$$
$$\dot{e}_y = -K_{p,y}e_y - K_{i,y}\int e_y\,dt$$

When we consider the disturbances as well, we get:

$$\dot{e}_x + K_{p,x}e_x + K_{i,x}\int e_x\,dt = d$$
$$\dot{e}_y + K_{p,y}e_y + K_{i,y}\int e_y\,dt = d$$

If we differentiate these error terms one more time we get:

$$\ddot{e}_x + K_{p,x}\dot{e}_x - K_{i,x}e_x = \dot{d}$$
$$\ddot{e}_y + K_{p,y}\dot{e}_y - K_{i,y}e_y = \dot{d}$$

In the steady state, error terms behave as:

$$e_x \to c$$
$$\dot{e}_x \to 0$$
$$\ddot{e}_x \to 0$$

As a result, we have:

$$\begin{aligned} 0+0+K_i c &= \dot{d} \\ c &\approx \frac{\dot{d}}{K_i} \end{aligned}$$

This demonstrates that, for gradually varying disturbances, the steady-state error asymptotically converges to zero. Finally, by combining the results obtained thus far, we construct the first virtual control input u_1. From Eq. 4.1 and Eq. 4.2, we obtain:

$$\begin{aligned} \dot{x} &= u_1 \cos\theta = \mu_x \\ \dot{y} &= u_1 \sin\theta = \mu_y \end{aligned}$$

With some basic trigonometric manipulation, we obtain:

$$\begin{aligned} \sqrt{\mu_x^2 + \mu_y^2} &= \sqrt{(u_1\cos\theta)^2 + (u_1\sin\theta)^2} \\ &= \sqrt{u_1^2(\cos^2\theta + \sin^2\theta)} \\ &= u_1 \end{aligned}$$

The virtual input u_1 is:

$$u_1 = \sqrt{\mu_x^2 + \mu_y^2} \tag{4.4}$$

After obtaining u_1, we generate the desired angle input for the attitude controller:

$$\frac{\mu_y}{\mu_x} = \frac{u_1 \sin\theta}{u_1 \cos\theta} \tag{4.5}$$

Which becomes:

$$\tan\theta = \frac{\mu_y}{\mu_x} \tag{4.6}$$

The desired heading angle which will be fed to the attitude controller is:

$$\theta_d = \text{atan2}(\mu_y, \mu_x) \tag{4.7}$$

Attitude Control

Once u_1 and the desired heading angle are determined, the attitude controller acts to drive the orientation error to zero. As before, virtual control inputs of the PID type are employed. The error dynamics for the attitude are defined as follows:

$$e_\theta = \theta_d - \theta \tag{4.8}$$
$$\dot{e}_\theta = \dot{\theta}_d - \dot{\theta} \tag{4.9}$$

Analogous to the synthesis of u_1, the virtual input μ_θ is chosen as $\dot{\theta}$. To eliminate the need for derivative information, a feedforward term is incorporated alongside PI control terms, yielding:

$$\mu_\theta = \dot{\theta}_d + K_{p,\theta} \cdot e_\theta + K_{i,\theta} \int e_\theta \, dt \tag{4.10}$$

The term $\dot{\theta}_d$ is obtained by differentiating Equation (4.7).

$$\left(1 + \tan^2 \theta\right) \dot{\theta}_d = \frac{\dot{\mu}_y \mu_x - \dot{\mu}_x \mu_y}{\mu_x^2} \tag{4.11}$$

Which is equal to:

$$\left(1 + \frac{\mu_y^2}{\mu_x^2}\right) \dot{\theta}_d = \frac{\dot{\mu}_y \mu_x - \dot{\mu}_x \mu_y}{\mu_x^2} \tag{4.12}$$

Which further simplifies to:

$$\dot{\theta}_d = \frac{\dot{\mu}_y \mu_x - \dot{\mu}_x \mu_y}{\mu_x^2 + \mu_y^2} \tag{4.13}$$

Following these derivations, the virtual input μ_θ can now be fully determined. Since the second virtual input and the orientation control input were selected as the derivative of the heading angle in Eq. 4.3 and Eq. 4.7, respectively, the second control input is given by:

$$u_2 = \mu_\theta \tag{4.14}$$

4.2. Modeling and Motion Control of Fixed Wing UAVs

Following the UGV case studies in 2D space, we address the primary challenge of this work: tracking a moving target in three-dimensional space using fixed-wing UAVs. This scenario closely represents the real-world multi-UAV aerial refueling rendezvous problem that motivates this research. As such, the examples in this section form the core of the problem formulation. The preceding sections serve as foundational preparation for the autonomous rendezvous of multiple fixed-wing UAVs.

4.2.1. Equations of Motion for Fixed Wing UAVs

Having arrived at the central scenario, this section focuses on fixed-wing UAV models. Specifically, the six degrees-of-freedom (6-DOF) dynamic equations governing the motion of fixed-wing aircraft are presented and discussed.

Coordinate Frames

We define two coordinate frames:

- **Inertial frame (Earth frame)**: (X, Y, Z)
- **Body frame (attached to the UAV CG)**: (x, y, z), where:
  - x: forward
  - y: right
  - z: downward

State Variables

- **Position in inertial frame:** $\mathbf{p} = [x, y, z]^T$
- **Linear velocity in body frame:** $\mathbf{v} = [u, v, w]^T$
- **Orientation (Euler angles):** $\boldsymbol{\eta} = [\phi, \theta, \psi]^T$ (roll, pitch, yaw)
- **Angular velocity in body frame:** $\boldsymbol{\omega} = [p, q, r]^T$

Translational Dynamics

Newton's second law in the body frame:

$$m\dot{\mathbf{v}} + \boldsymbol{\omega} \times (m\mathbf{v}) = \mathbf{F}_{\text{body}}$$

Component-wise:

$$\begin{bmatrix} \dot{u} \\ \dot{v} \\ \dot{w} \end{bmatrix} = \frac{1}{m} \begin{bmatrix} X \\ Y \\ Z \end{bmatrix} - \begin{bmatrix} qw - rv \\ ru - pw \\ pv - qu \end{bmatrix}$$

Where X, Y, Z are total external forces in the body frame.

Rotational Dynamics

Euler's equations for rotational motion:

$$\mathbf{I}\dot{\boldsymbol{\omega}} + \boldsymbol{\omega} \times (\mathbf{I}\boldsymbol{\omega}) = \boldsymbol{M}$$

$$\begin{bmatrix} \dot{p} \\ \dot{q} \\ \dot{r} \end{bmatrix} = \mathbf{I}^{-1} \left(\begin{bmatrix} L \\ M \\ N \end{bmatrix} - \boldsymbol{\omega} \times (\mathbf{I}\boldsymbol{\omega}) \right)$$

Where $\mathbf{I}$ is the inertia matrix and L, M, N are control moments.

Kinematic Equations

Translational Kinematics (position update in inertial frame):

$$\begin{bmatrix} \dot{x} \\ \dot{y} \\ \dot{z} \end{bmatrix} = R(\phi, \theta, \psi) \begin{bmatrix} u \\ v \\ w \end{bmatrix}$$

Euler Angle Rates:

$$\begin{bmatrix} \dot{\phi} \\ \dot{\theta} \\ \dot{\psi} \end{bmatrix} = \begin{bmatrix} 1 & \sin\phi\tan\theta & \cos\phi\tan\theta \\ 0 & \cos\phi & -\sin\phi \\ 0 & \sin\phi/\cos\theta & \cos\phi/\cos\theta \end{bmatrix} \begin{bmatrix} p \\ q \\ r \end{bmatrix}$$

Aerodynamic Forces and Moments

Forces:

$$X = -D + T \quad \text{(drag and thrust)}$$
$$Y = \text{sideslip force}$$
$$Z = -L \quad \text{(lift)}$$

Moments:

$$\boldsymbol{M} = \begin{bmatrix} L \\ M \\ N \end{bmatrix}$$

Generated by control surfaces (aileron, elevator, rudder) and aerodynamic effects.

4.2.2. Trajectory Tracking Control for Fixed Wing UAVs

To simplify the trajectory tracking problem for fixed-wing UAVs, we employed the MATLAB UAV Toolbox, which offers a comprehensive set of tools for guidance, navigation, and control, as well as for simulating the dynamics of aerial vehicles. This toolbox is particularly useful for prototyping control systems and validating their performance in a modular and visual manner. The overall control architecture, which integrates trajectory generation, way-point management, and flight control, is illustrated in Fig. 4.4.

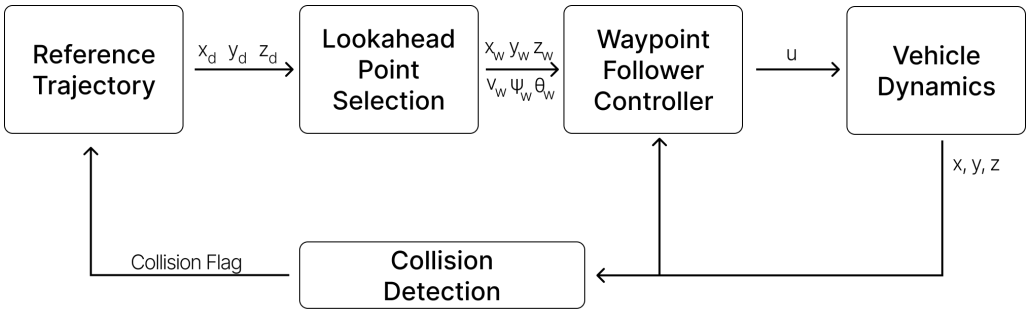

Figure 4.4 Way-point follower controller structure

The process begins with the generation of a reference trajectory. This is defined as a sequence of 3D way-points derived from the high-level planner. These way-points encode spatial information (x, y, z) and can also be used to derive associated parameters such as desired yaw (heading) and airspeed, both of which are essential

for control. The trajectory data is then sub-sampled, which structures the look-ahead points.

Trajectory tracking is achieved using the Way-point Follower block, which is based on a pure pursuit guidance strategy. In this method, the UAV continuously aims at a dynamically selected look-ahead point on the path. This look ahead point moves along the trajectory, effectively pulling the UAV toward the path in a smooth and stable manner. Once a way-point is reached—typically determined by a proximity threshold—the controller switches its target to the next way-point in the sequence. This creates a cascaded tracking behavior where the UAV advances from one way-point to the next until the entire trajectory is completed.

The look-ahead concept is crucial to this approach. Rather than reacting to the immediate next way-point, the controller projects forward along the path to a point at a fixed distance ahead. This anticipatory behavior improves stability and reduces oscillations, especially at higher speeds. The look-ahead distance can be tuned based on the UAV's dynamics and mission requirements to strike a balance between responsiveness and smoothness.

For flight control, the system utilizes a simplified control structure that abstracts away the complexity of individual actuator dynamics. Instead of directly commanding control surfaces like ailerons, elevators, or rudders, the controller operates on higher-level control variables: roll angle, altitude, and airspeed. These are interpreted respectively as the outputs of inner-loop PID controllers that drive the aircraft using the appropriate combinations of control surfaces. The MATLAB UAV Toolbox provides pre-configured PID-based control blocks for these inputs, significantly reducing development complexity while still capturing essential control behavior.

This abstraction not only streamlines the simulation process but also makes the control system more robust and easier to tune. By operating at this higher level, the model avoids the need for detailed low-level actuator modeling, making it more accessible for rapid prototyping and algorithm testing.

In summary, the trajectory tracking system is composed of three main components: (1) the way-point generation block that structures trajectory data and derives necessary inputs, (2) the way-point follower implementing pure pursuit logic with a lookahead point, and (3) the control system that converts tracking errors into roll, altitude, and airspeed commands. This architecture leverages the capabilities of MATLAB's UAV Toolbox to provide a flexible yet powerful platform for developing and testing guidance and control algorithms for fixed-wing UAVs.

5. RESULTS AND DISCUSSION

Computer simulations were conducted to evaluate the performance of the proposed schemes in both 2D and 3D environments. Initially, proof-of-concept scenarios involving unmanned ground vehicles (UGVs) in 2D space were tested. After obtaining promising results, the framework was extended to the more complex 3D environment using fixed-wing unmanned aerial vehicles (UAVs), which was the ultimate goal of this work. Satisfactory results were achieved in both domains.

All simulations were carried out in the MATLAB/Simulink environment. A multi-vehicle system was modeled to perform a coordinated task: approaching a target within a defined proximity. The framework was tested with three vehicles in both the 2D UGV and 3D UAV scenarios. Each case was linked to real-world analogues and followed by a brief discussion.

To evaluate the effectiveness and robustness of the proposed methods, three main scenarios were developed:

- 2D with a static target
- 2D with a dynamic target
- 3D with a dynamic target

For each scenario, a case study is presented, beginning with a brief description followed by a presentation and analysis of the results. We examine the reference and actual trajectories of each vehicle, analyze the error characteristics, and present the corresponding control inputs. Additional performance metrics are also visualized to provide deeper insight into the behavior of the trajectory generation and tracking control components.

5.1. 2D Results with UGVs

In this section, we examine two scenarios involving non-holonomic, differential-drive UGV groups: one with a stationary target and the other with a moving target.

Scenario 1

The first scenario considers a 2D environment with a stationary target. This setup is analogous to real-world situations such as a platoon of autonomous ground vehicles (UGVs) reaching a destination or returning to base. In this case, the reference trajectory is shaped by three main components: an attractive force toward the target, repulsive forces between vehicles, and a collision avoidance mechanism.

Vehicles advance toward the target while exerting repelling forces on each other to maintain spacing. However, beyond a predefined distance, these repelling forces are deactivated to reduce computational load and avoid unnecessary constraints. This simplification improves real-time trajectory generation and enables more efficient path planning.

Table 5.1 Scenario-1 simulation parameters

Parameter	Value
$m\ (kg)$	1
$b\ (N/m)$	8
$k\ (Ns/m)$	9
$r_{goal}\ (m)$	0.6
$k_{rep}\ (Nm^2)$	2
$r_{rep}\ (m)$	0.8
$d_{critical}\ (m)$	0.4
c_{rep}	1.5
c_{slow}	0.8

Key parameters given in Tab. 5.1 influencing the system's behavior include:

- m, b, k: mass, damping, and spring coefficients used in the high-level planner
- r_{goal}: minimum allowable distance from the target that vehicles aim to reach
- k_{rep}, r_{rep}: coefficient and maximum effective range of repulsive forces between vehicles
- d_{critical}: distance threshold that triggers the collision avoidance mechanism
- c_{rep}: scaling factor that amplifies the repulsive force when a potential collision is detected
- c_{slow}: scaling factor that reduces the spring coefficient of the more distant vehicle during potential collision scenarios

Trajectory plots shown in Fig. 5.1 use red, green, and blue lines to represent UGV-1, UGV-2, and UGV-3, respectively. Dashed lines show the reference paths, while solid lines depict the actual trajectories. The target is marked with a cyan star, and the minimum allowable distance to the target is indicated by a magenta circle.

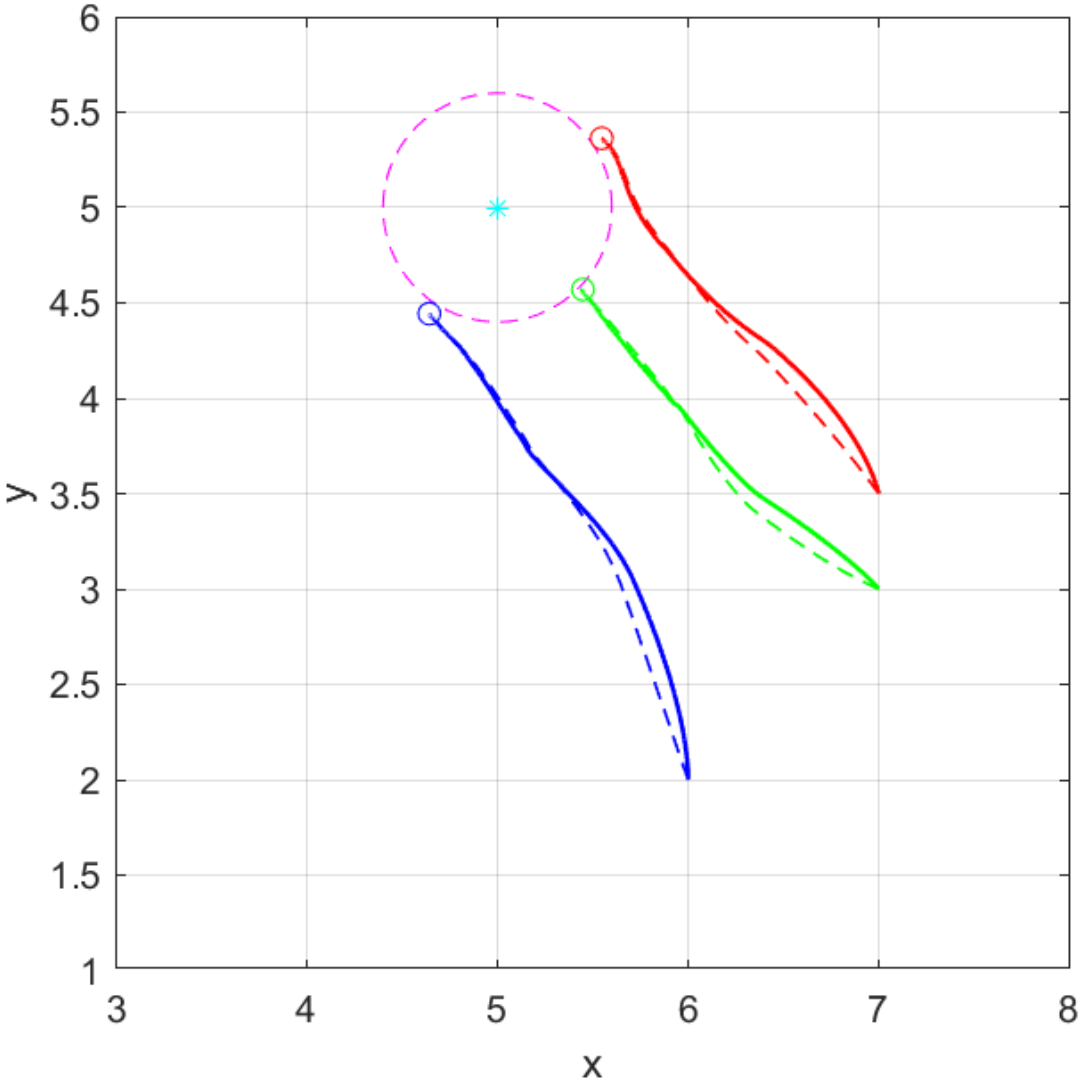

Figure 5.1 UGV trajectories of Scenario-1

The vehicles closely follow their respective reference trajectories and converge rapidly toward the target. No specific formation is enforced during the approach to prioritize path efficiency. However, due to mutual repulsion, the vehicles eventually distribute themselves uniformly around the target.

Tracking Error Analysis

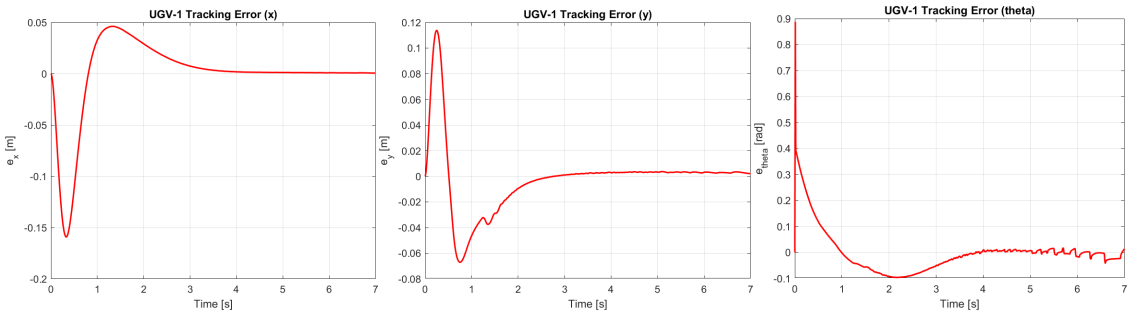

(a) (b) (c)

Figure 5.2 Tracking errors of UGV-1

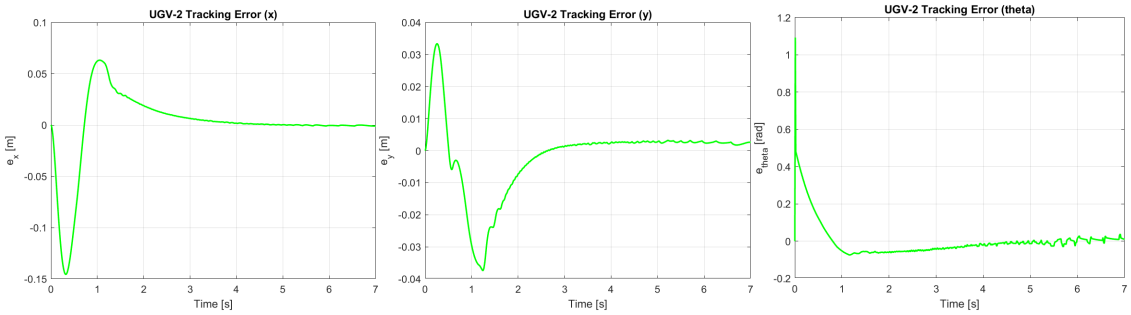

(a) (b) (c)

Figure 5.3 Tracking errors of UGV-2

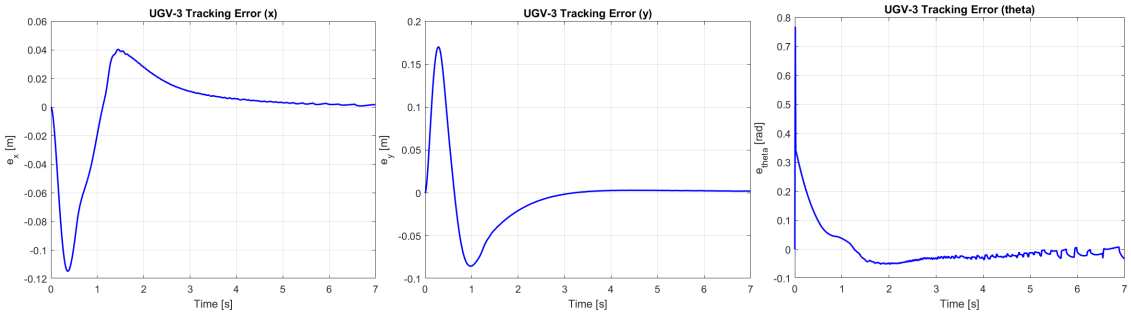

(a) (b) (c)

Figure 5.4 Tracking errors of UGV-3

In Figs. 5.2-5.4 it is shown that the positional tracking errors in both x and y directions given are minimal and decay quickly. Orientation errors exhibit an initial spike but then stabilize, although some jitter remains. This behavior is expected due to the cascaded structure of the controller: the outer loop controls position, while the inner loop adjusts orientation based on positional demands. The controller prioritizes minimizing x and y errors, which often requires abrupt changes in heading.

To quantitatively assess tracking performance, tracking errors are summarized in tabular form using maximum and root mean square (RMS) values.

Table 5.2 Tracking errors of UGV-1

Tracking Error	max(abs)	RMS
e_x (m)	0.1592	0.0381
e_y (m)	0.1138	0.0274
e_θ (rad)	0.8879	0.0862

Table 5.3 Tracking errors of UGV-2

Tracking Error	max(abs)	RMS
e_x (m)	0.1457	0.0355
e_y (m)	0.0374	0.0118
e_θ (rad)	1.0930	0.0964

Table 5.4 Tracking errors of UGV-3

Tracking Error	max(abs)	RMS
e_x (m)	0.1147	0.0310
e_y (m)	0.1703	0.0416
e_θ (rad)	0.7690	0.0706

The data in Tabs. 5.2-5.4 confirms that orientation errors are generally larger than positional ones, as seen in the RMS values. For example, UGV-2 shows a spike in orientation error toward the end of its maneuver. This occurs because even a minor overshoot near the target can cause a sudden change in the reference orientation, resulting in a significant heading discrepancy, despite the vehicle being spatially accurate.

Control Input Analysis

The UGV controller utilizes two control inputs:

- u_1: Governs linear motion
- u_2: Governs rotational motion (heading/orientation)

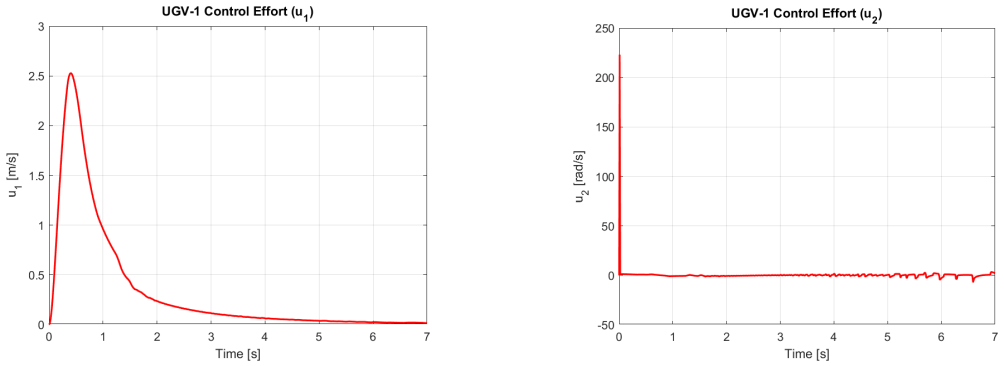

(a) (b)

Figure 5.5 Control inputs of UGV-1

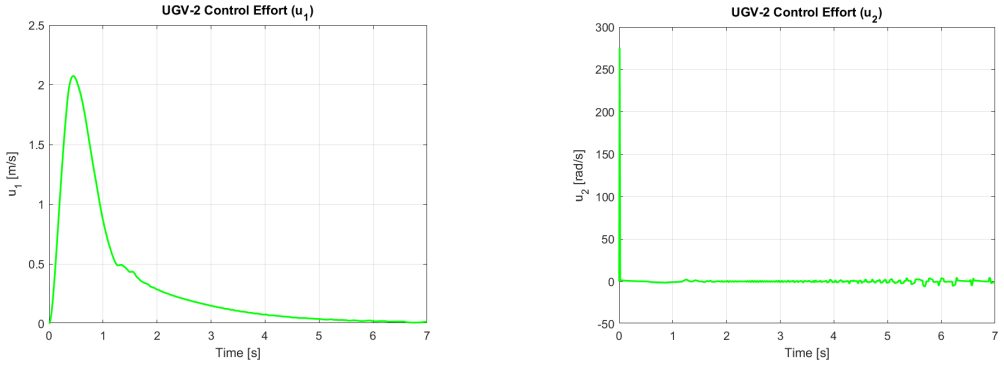

(a) (b)

Figure 5.6 Control inputs of UGV-2

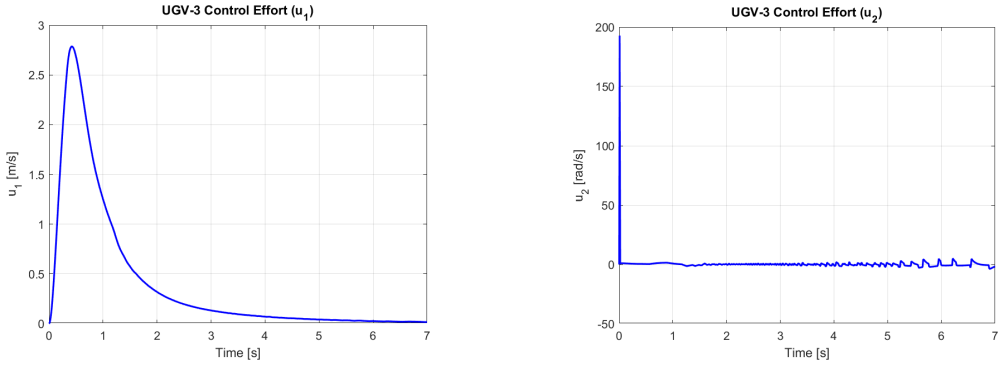

(a) (b)

Figure 5.7 Control inputs of UGV-3

As seen in Figs. 5.5-5.7 ,the u_1 input exhibits an initial peak followed by smooth convergence, reflecting the behavior of the positional errors. In contrast, u_2 tends to be more jittery, frequently adjusting to meet orientation demands.

Table 5.5 Control inputs of UGV-1

Control Effort	max(abs)	RMS
u_1 (m/s)	2.5275	0.6792
u_2 (rad/s)	223.1191	8.4853

Table 5.6 Control inputs of UGV-2

Control Effort	max(abs)	RMS
u_1 (m/s)	2.0742	0.5983
u_2 (rad/s)	275.7303	10.4963

Table 5.7 Control inputs of UGV-3

Control Effort	max(abs)	RMS
u_1 (m/s)	2.7864	0.7909
u_2 (rad/s)	192.7907	7.3712

To further quantify the results, we present the tracking error and control input data in Tabs. 5.5-5.7 including their maximum and root mean square (RMS) values. These metrics reinforce our previous observations: the position errors, e_x and e_y, remain consistently low. While the attitude error is comparatively larger, it remains within a tolerable range. Similarly, the control inputs reflect this trend: u_1, associated with position control, demonstrates stable and efficient behavior, whereas u_2, responsible for heading control, exhibits relatively higher variability.

Scenario 2

In the second scenario, the group again consists of three non-holonomic UGVs; the key difference is that the target moves linearly at a constant speed. This scenario models a UGV group pursuing a target during a reconnaissance mission or following a friendly agent. As the target's position changes, the reference trajectories dynamically update in real time, continuously adjusting to track the moving target.

The parameters remain largely the same as seen in Tab. 5.8, except for an increased d_{critical} to amplify the repulsion effect for clearer observation. Additionally, the vehicles start closer together than in the previous scenario. This causes an initial scattering behavior, confirming that the repulsion mechanism is effectively activated. Subsequently, the vehicles maintain balanced spacing and successfully track the dynamic target, whose trajectory during the operation is shown by the dashed black line.

Table 5.8 Scenario-2 simulation parameters

Parameter	Value
$m\ (kg)$	1
$b\ (N/m)$	8
$k\ (Ns/m)$	9
$r_{goal}\ (m)$	0.6
$k_{rep}\ (Nm^2)$	2
$r_{rep}\ (m)$	0.8
$d_{critical}\ (m)$	0.6
c_{rep}	1.5
c_{slow}	0.8

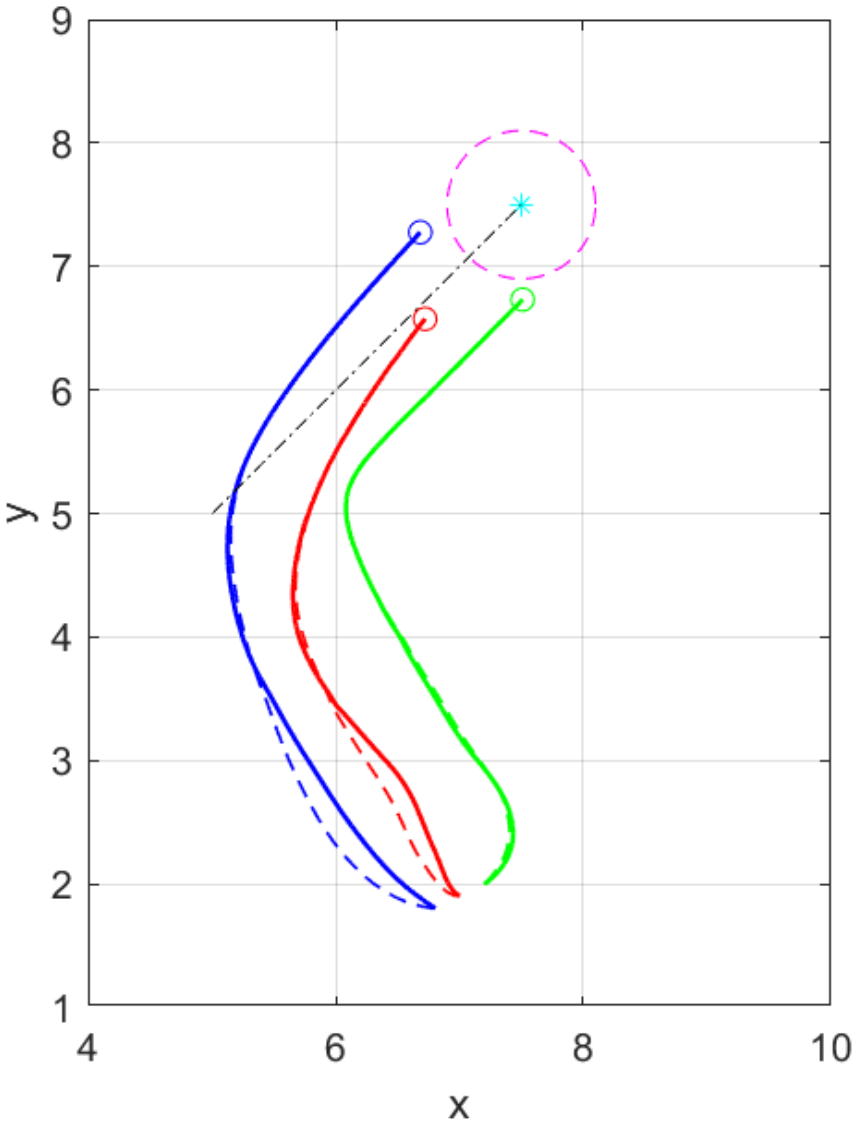

Figure 5.8 UGV trajectories of Scenario-2

We observe in Fig. 5.8 that the high-level planner generates efficient trajectories despite the continuous movement of the target. Furthermore, the vehicle group follows these desired paths with high accuracy, demonstrating the effectiveness of both trajectory generation and tracking. To gain deeper insight, we proceed with a detailed analysis of the error dynamics.

Tracking Error Analysis

Similar to Scenario 1, the UGVs successfully track their respective reference trajectories. To evaluate tracking performance, we plot the errors in x, y, and θ over time and analyze their behavior in Figs. 5.9-5.11.

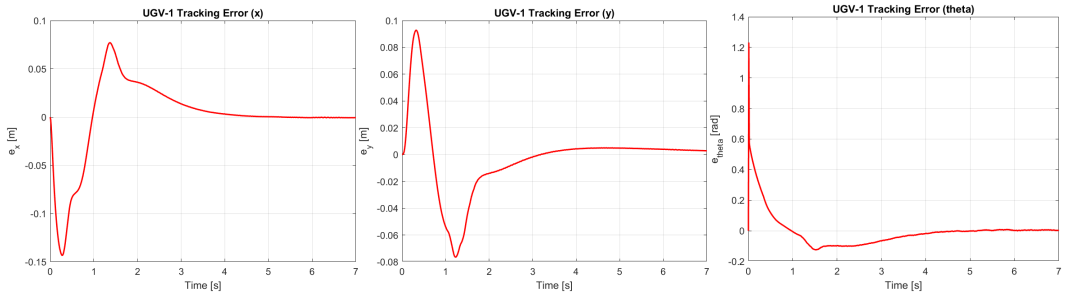

(a) (b) (c)

Figure 5.9 Tracking errors of UGV-1

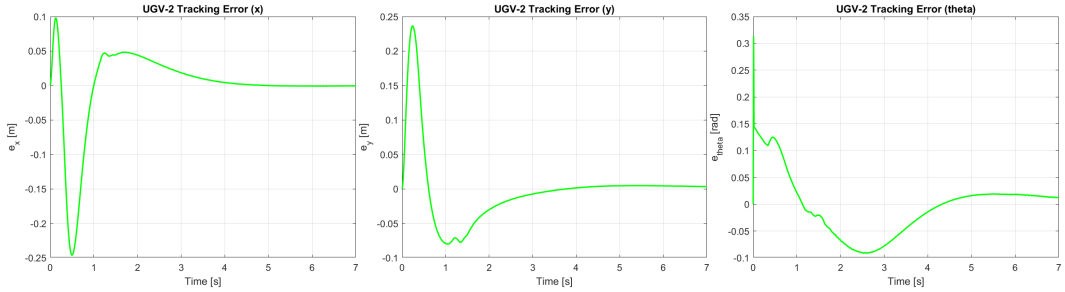

(a) (b) (c)

Figure 5.10 Tracking errors of UGV-2

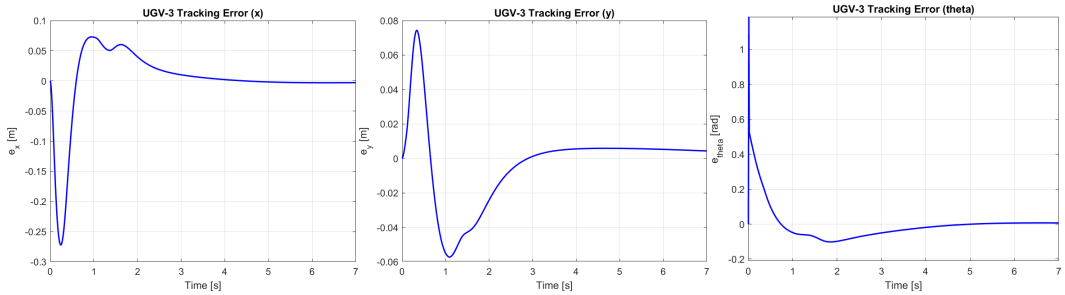

(a) (b) (c)

Figure 5.11 Tracking errors of UGV-3

As in the stationary target scenario, the UGVs effectively track their trajectories when pursuing a moving target. The tracking errors in x and y exhibit a slight initial peak but quickly diminish and converge to zero. These results indicate that the UGVs maintain strong position tracking performance in both stationary and moving target cases.

Table 5.9 Tracking errors of UGV-1

Tracking Error	max(abs)	RMS
e_x (m)	0.1434	0.0395
e_y (m)	0.0928	0.0278
e_θ (rad)	1.2318	0.1125

Table 5.10 Tracking errors of UGV-2

Tracking Error	max(abs)	RMS
e_x (m)	0.2461	0.0560
e_y (m)	0.2365	0.0533
e_θ (rad)	0.3134	0.0574

Table 5.11 Tracking errors of UGV-3

Tracking Error	max(abs)	RMS
e_x (m)	0.2721	0.0579
e_y (m)	0.0743	0.0242
e_θ (rad)	1.1991	0.1045

Results in Tabs. 5.9-5.11 once again support our initial observations, showing small and rapidly decaying errors across all metrics. Even the orientation error yields a satisfactory RMS value, with only the maximum value indicating occasional sharp changes in heading angle.

Control Input Analysis

As in the previous scenario, u_1 and u_2 serve as the control inputs. When plotted, they exhibit behavior similar to that observed in Scenario 1.

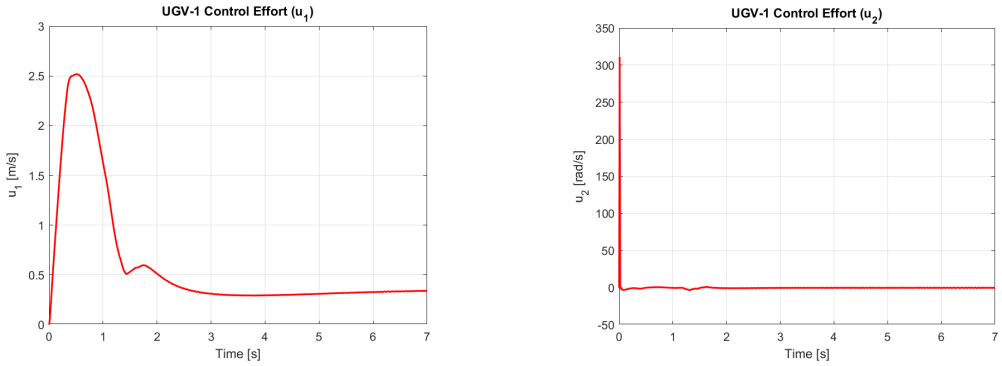

(a) (b)

Figure 5.12 Control inputs of UGV-1

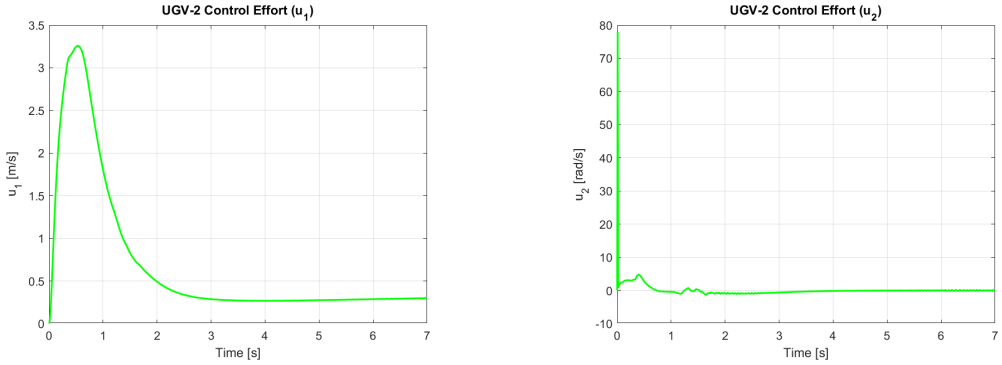

(a) (b)

Figure 5.13 Control inputs of UGV-2

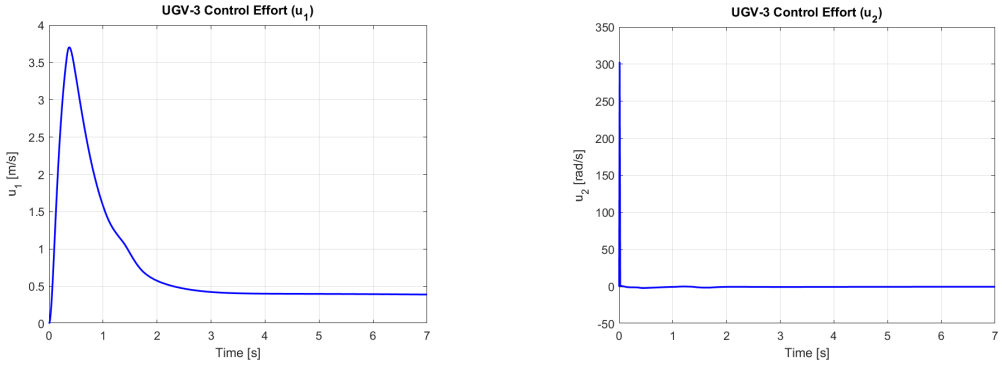

(a) (b)

Figure 5.14 Control inputs of UGV-3

As observed in Figs. 5.12-5.14, the control input u_1 exhibits a slight initial peak before gradually decaying. Similarly, u_2 begins with a sharp change but stabilizes quickly. The remaining jitter in u_2, as discussed earlier, is an expected consequence of the controller's cascaded structure.

Table 5.12 Control inputs of UGV-1

Control Effort	max(abs)	RMS
u_1 (m/s)	2.5174	0.8753
u_2 (rad/s)	311.0981	11.7691

Table 5.13 Control inputs of UGV-2

Control Effort	max(abs)	RMS
u_1 (m/s)	3.2587	1.0806
u_2 (rad/s)	77.9883	3.1106

Table 5.14 Control inputs of UGV-3

Control Effort	max(abs)	RMS
u_1 (m/s)	3.7030	1.1043
u_2 (rad/s)	303.0721	11.4570

Similar to the previous case, Tabs. 5.12-5.14 show that the control effort u_2 is significantly larger and more variable, while u_1 remains relatively smooth. However, a key difference from the stationary target scenario is the overall increase in the magnitude of both control inputs. This is a direct consequence of the dynamic nature of pursuing a moving target. Despite the increased demands, tracking performance remains strong—achieved through greater control effort.

5.2. 3D Results with UAVs

Scenario 3

This scenario reflects the primary motivation of this study: coordinating multiple fixed-wing unmanned aerial vehicles (UAVs) during a rendezvous phase with a fuel tanker traveling at a constant velocity. Specifically, three UAVs are tasked with approaching a moving target (the tanker), starting from arbitrary initial positions, orientations, and velocities. At the beginning of the operation, the UAVs attempt to converge on the tanker's path, which results in a brief clustering behavior. Due to the quadratic nature of the virtual repelling forces, this close proximity leads to a significant increase in repulsion, causing the UAVs to spread out and establish more stable distances while continuing to follow the tanker.

This simulation models a typical mid-mission refueling scenario. In practice, such operations would require prior planning to ensure a tanker aircraft is available near the estimated refueling time. These requirements can be pre-calculated or dynam-

ically adjusted during the mission. It is assumed that the UAVs are capable of inter-vehicle communication, and that the tanker broadcasts its position and velocity. This minimal information sharing is sufficient to carry out the coordination.

Once communication is established, each UAV independently plans its trajectory toward the tanker using a decentralized control approach, as discussed in earlier sections of this manuscript. As they navigate toward the moving target, the UAVs coordinate to avoid collisions—either by applying gentle repulsion or, in critical cases, by deferring to the nearer vehicle. After a period of pursuit and stabilization, the system transitions into a second phase, in which the UAVs align at the same altitude, side by side. Wider vehicles naturally occupy outer positions.

Table 5.15 Scenario-3 simulation parameters

Parameter	Value
$m\ (kg)$	100
$b\ (N/m)$	70
$k\ (Ns/m)$	30
$r_{goal}\ (m)$	10
$k_{rep}\ (Nm^2)$	$1.5 \cdot 10^5$
$r_{rep}\ (m)$	50
$d_{critical}\ (m)$	20
c_{rep}	1.5
c_{slow}	0.7
$d_{safe}\ (m)$	20
$d_{dock}\ (m)$	200

In addition to the initial rendezvous, this scenario includes a second phase: the pre-docking stage. While most parameters remain consistent with previous examples, two additional ones are introduced in Tab. 5.15: d_{safe} and d_{dock}. These define the minimum safe separation between UAVs and the required distance between the receivers and the tanker, respectively. Once both conditions are met, the system transitions into the second phase. During this phase, the attraction points are dynamically adjusted to guide the UAVs into a formation flight on the same horizontal plane, in preparation for docking. Specifically, the UAVs on the left and right begin to align with refueling probes located along the wings of the tanker. As the attraction centers shift, these UAVs are directed toward the wing tips rather than the tanker's center of mass. The final formation positions all three UAVs correctly and in close proximity, ready to initiate aerial refueling.

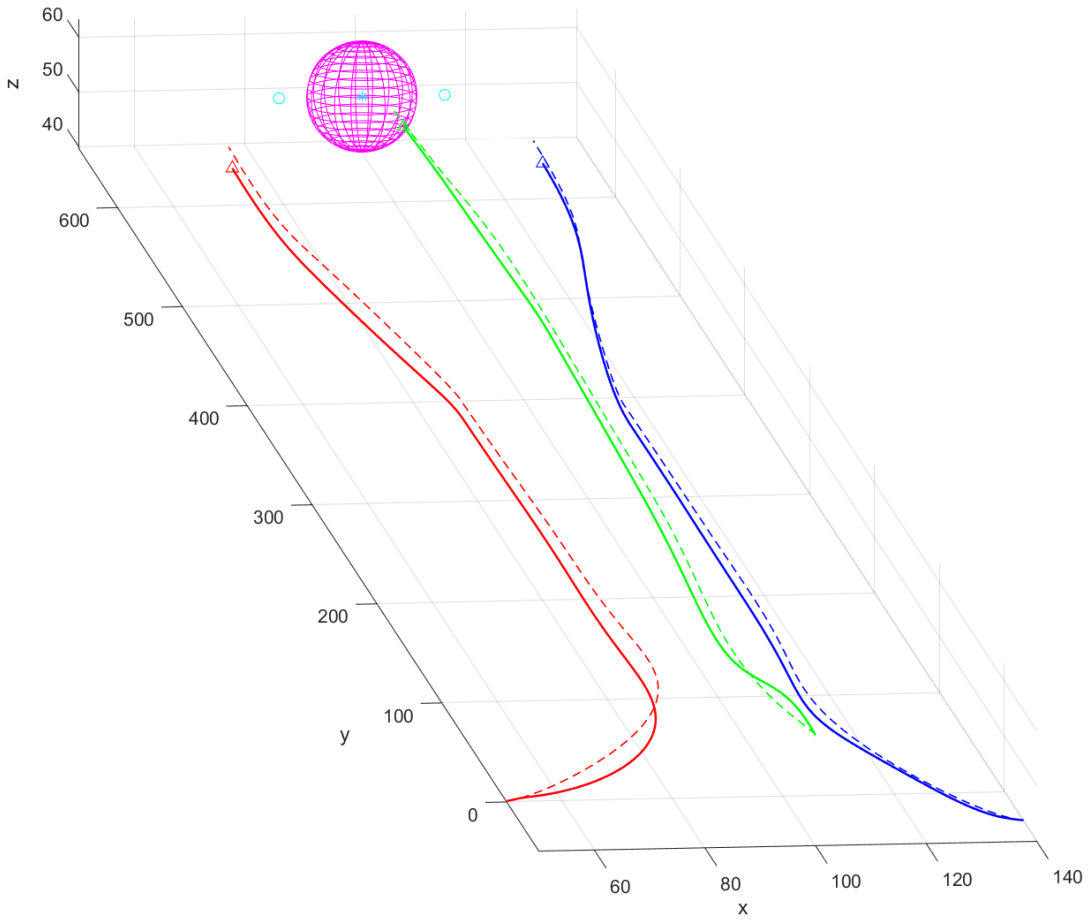

Figure 5.15 UAV trajectories of Scenario-3

The UAV trajectories are shown in Fig. 5.15, where the red, green, and blue lines represent UAVs 1, 2, and 3, respectively. The target (tanker) is indicated by a cyan star, and the magenta sphere denotes the minimum separation radius each UAV must maintain during the approach. The simulation demonstrates successful execution of the operation. To further assess performance, we proceed to analyze the error dynamics and control inputs.

Tracking Error Analysis

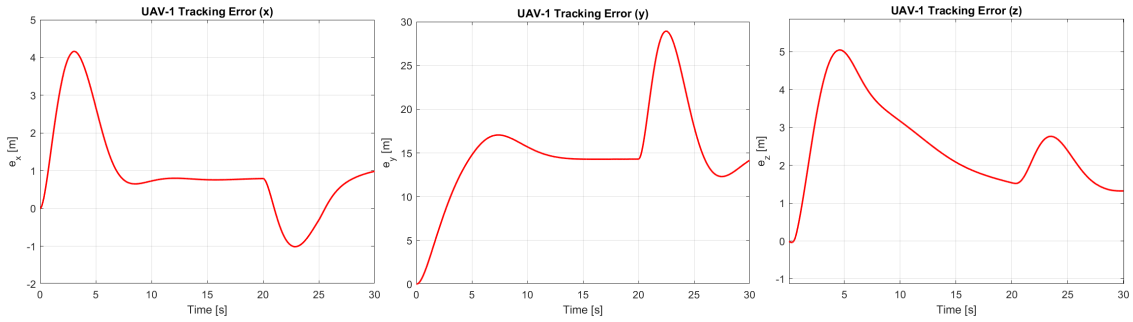

(a) (b) (c)

Figure 5.16 Tracking errors of UAV-1

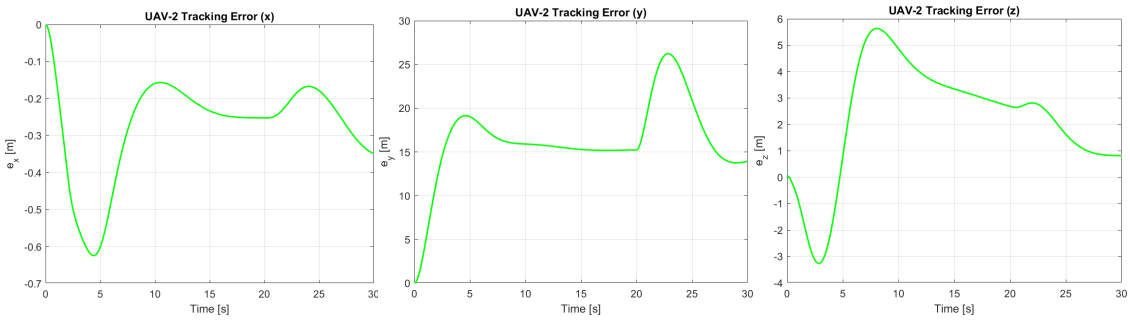

(a) (b) (c)

Figure 5.17 Tracking errors of UAV-2

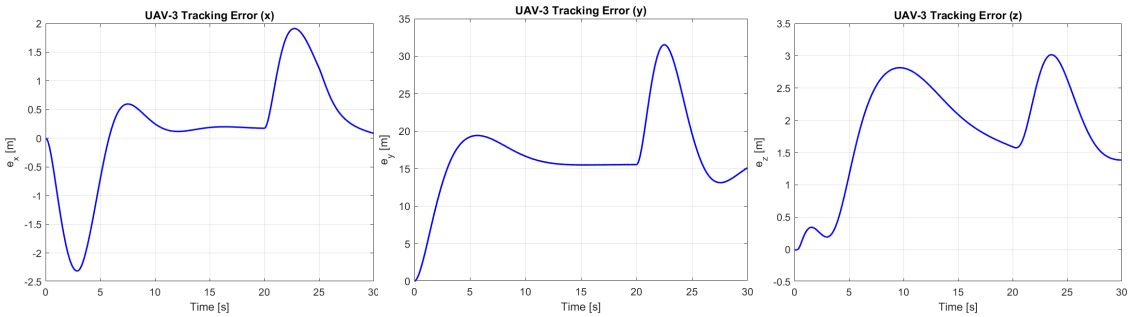

(a) (b) (c)

Figure 5.18 Tracking errors of UAV-3

Analyzing the tracking error dynamics in Figs. 5.16-5.18, the x-direction stands out with high accuracy. Given the scale of the aircraft models used, the results are quite satisfactory. The z-direction (altitude) error also performs reasonably well, gradually diminishing over time—an acceptable outcome considering the dimensions of used models (approximately 9 m in length and 13 m in wingspan).

However, the e_y error appears less favorable. This initially seems inconsistent with the reference vs. actual trajectory plots, which suggest good overall tracking performance. The key nuance lies in the interpretation of the y-axis: it corresponds to the forward motion of the target. Therefore, an error in this direction indicates a lag in forward progress rather than spatial deviation. In other words, the UAVs follow the correct path but trail slightly behind the reference trajectory.

This highlights a critical distinction in trajectory tracking: while a path defines spatial position alone, a trajectory also incorporates timing. Falling behind in the y-direction implies a temporal mismatch, not necessarily a spatial error.

The primary reason for this lag is the use of airspeed as a control input for the receiver UAVs. When a delay occurs, the vehicles cannot easily accelerate to "catch up" because they are also constrained to maintain specific speed profiles. As a result,

the y-axis error grows larger—not due to deviation from the planned route, but due to timing misalignment. This lag first increases then decreases during the second phase, as the reference speed grows larger first but then UAVs catch up, stabilize and complete the formation.

Table 5.16 Tracking errors of UAV-1

Tracking Error	max(abs)	RMS
e_x (m)	4.1636	1.5075
e_y (m)	28.9203	15.9556
e_z (m)	5.0480	2.7668

Table 5.17 Tracking errors of UAV-2

Tracking Error	max(abs)	RMS
e_x (m)	0.6245	0.3034
e_y (m)	26.2299	16.9733
e_z (m)	5.6334	3.1262

Table 5.18 Tracking errors of UAV-3

Tracking Error	max(abs)	RMS
e_x (m)	2.3150	0.9519
e_y (m)	31.5329	17.7744
e_z (m)	3.0168	2.0416

Tabs. 5.16-5.18 further confirm our observations from the plots: both e_x and e_z remain relatively low, while the e_y errors are noticeably larger. However, as previously discussed, this increase in e_y is expected and can be attributed to the temporal lag in the direction of motion. Interpreting the RMS and maximum error values together reveals an important insight: the maximum e_y errors are not significantly higher than the RMS values. This indicates a consistent error throughout the flight, rather than abrupt spikes that might pose operational risks. As explained earlier, this persistent error represents a steady lag rather than a deviation from the intended path. While it is evident in the error analysis, it does not compromise the safety or success of the mission.

Control Effort Analysis

In the UAV scenario, there are three control inputs shown in Figs. 5.19-5.21: u_{roll}, u_{altitude}, and u_{airspeed}. These inputs were introduced and discussed in detail in Chapter 4. In this section, we focus on evaluating their behavior and interpreting the corresponding results.

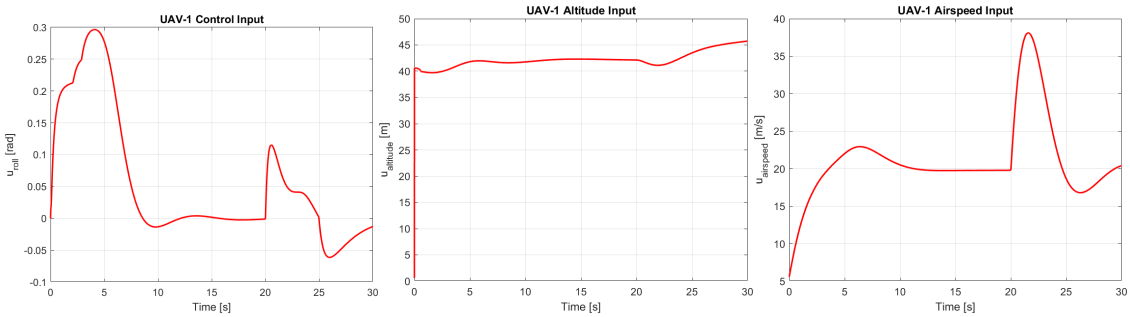

(a) Roll (b) Altitude (c) Airspeed

Figure 5.19 Control inputs of UAV-1

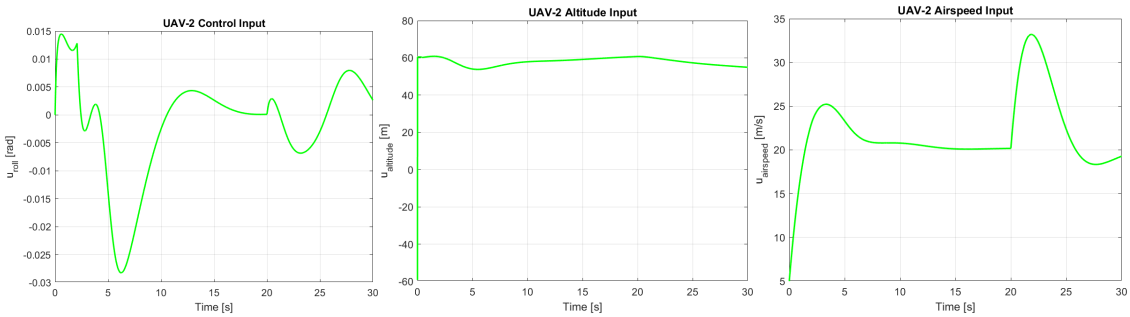

(a) Roll (b) Altitude (c) Airspeed

Figure 5.20 Control inputs of UAV-2

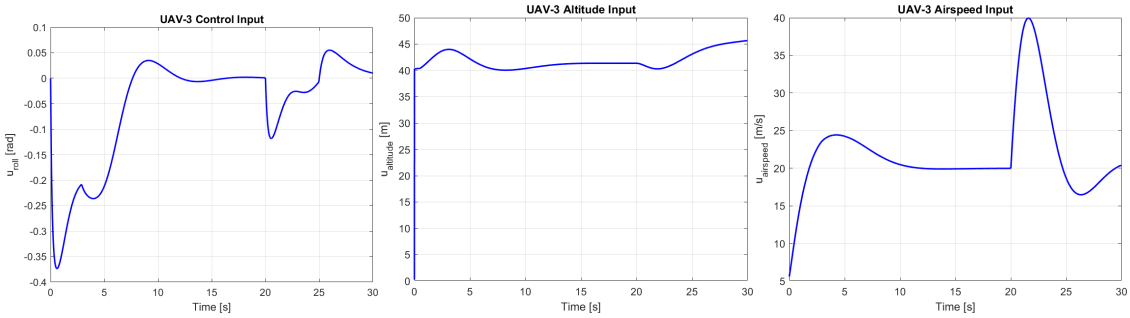

(a) Roll (b) Altitude (c) Airspeed

Figure 5.21 Control inputs of UAV-3

The roll control inputs are well within acceptable bounds. Although a saturation limit exists in the Simulink dynamic model, it was not reached at any point during this scenario. This indicates two key points: first, the generated reference trajectories are smooth and feasible; and second, the controller has been effectively tuned to track those trajectories without requiring aggressive control actions.

The altitude control input shows an initial spike, followed by a stable response. This early peak results from the discrepancy between the UAVs' initial altitudes

and the desired altitude. Notably, toward the end of the operation, UAV-2 descends while the other two ascend. This behavior is associated with the transition into the second phase of the operation. UAV-2 begins at a higher altitude, and due to repulsive interactions, the formation initially resembles a vertical triangle—with each UAV attracted toward the tanker's center and simultaneously pushed apart by mutual repulsion. When the second phase is triggered, the attraction centers shift to the refueling points along the tanker's wings. This change leads to a leveled formation flight, requiring UAV-2 to descend while the other two slightly climb to match the tanker's altitude as shown in Fig. 5.22.

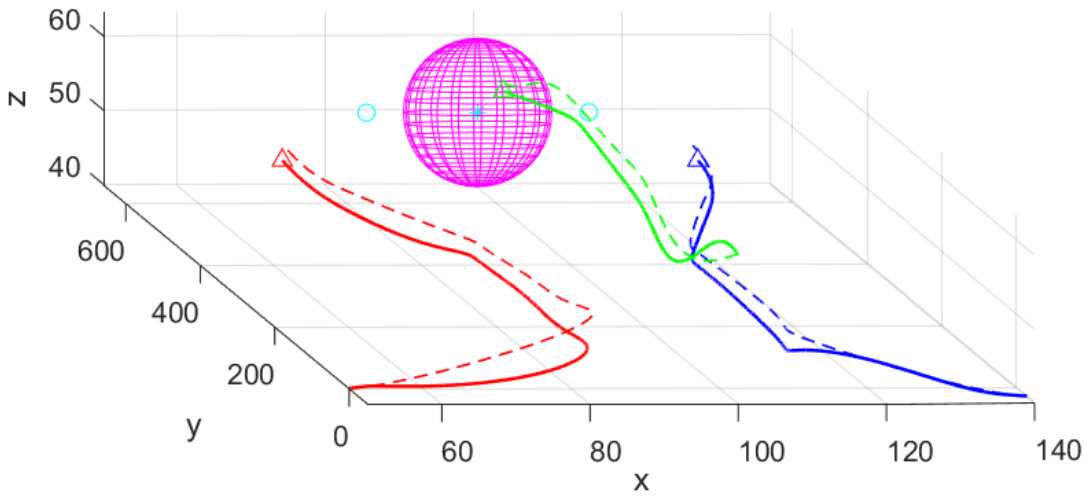

Figure 5.22 UAV altitudes converging

Airspeed inputs show a similar trend to the altitude control: an initial discrepancy leads to a stronger control effort at the start, followed by smooth and stable behavior. Toward the end of the operation, airspeed inputs increase again for all UAVs, which aligns with the initiation of the second phase. In this stage, the virtual spring coefficients are increased to reduce the distance between the UAVs and the tanker, resulting in higher airspeed demands and a corresponding acceleration response.

Table 5.19 Control inputs of UAV-1

Control Input	min(abs)	max(abs)	RMS
u_{roll} (rad)	0	0.2965	0.1155
$u_{altitude}$ (m)	0.6247	45.7405	42.2408
$u_{airspeed}$ (m/s)	5.5902	38.1206	21.7183

Table 5.20 Control inputs of UAV-2

Control Input	min(abs)	max(abs)	RMS
u_{roll} (rad)	0	0.0283	0.0093
$u_{altitude}$ (m)	53.8141	60.8514	58.0520
$u_{airspeed}$ (m/s)	5.0000	33.2051	22.1972

Table 5.21 Control inputs of UAV-3

Control Input	min(abs)	max(abs)	RMS
u_{roll} (rad)	0	0.3736	0.1183
$u_{altitude}$ (m)	0.2691	45.6763	41.9247
$u_{airspeed}$ (m/s)	5.5902	39.9588	22.5630

Tabs. 5.19-5.21 show that the roll control inputs align with expectations, exhibiting acceptable maximum values and promising RMS levels. When evaluating the altitude control input, it is important to note that its magnitude is relative to the cruise altitude; thus, a larger value does not necessarily indicate poor performance. A meaningful assessment involves comparing the RMS and maximum values, which in this case are reasonably close. The RMS values are also near the median target altitude—between 40m and 50m, depending on the UAV—indicating a well-balanced control effort.

In contrast, the airspeed input shows a more noticeable gap between the RMS and maximum values. This discrepancy is primarily due to the previously discussed "falling behind" phenomenon, in which the UAVs lag slightly in the direction of motion. Despite this, the RMS values remain close to the average desired airspeed, slightly above 20m/s.

Overall, the tabulated control input data is consistent with the trends observed in the plots, supporting the conclusions drawn from the system's performance.

3D Simulation using Unreal Engine

After obtaining the actual trajectories of each vehicle, we aimed to present the data in a more visually engaging and realistic manner through 3D simulations. To achieve this, a 3D visualization was developed using the *MATLAB UAV Toolbox*, which leverages the *Unreal Engine* for rendering. Below, several snapshots from the resulting 3D simulation video are provided to illustrate the outcome.

Figure 5.23 Receiver vehicles start to converge to the tanker

As shown in Fig. 5.23, the receivers, initially positioned at arbitrary locations and varying altitudes, begin to converge toward the tanker aircraft while maintaining a safe separation distance between each other.

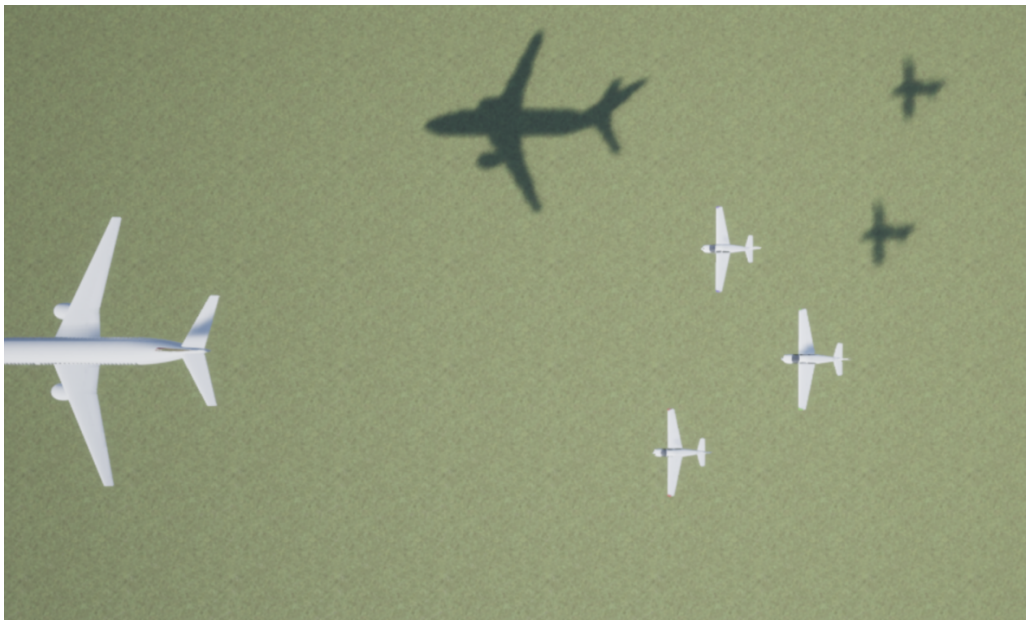

Figure 5.24 UAVs follow the tanker while forcing each other into a triangular formation

Fig. 5.24 demonstrates that, even in the absence of explicit formation constraints, the virtual attractive and repulsive forces naturally guide the group into a triangular configuration.

Figure 5.25 Final configuration

As shown in Fig. 5.25, the final configuration consists of one receiver positioned near the rear of the fuselage, while the other two are distributed near the wingtips.

In summary, the desired behavior is observed within the 3D simulation environment: attractive forces draw the receiver vehicles toward the tanker, while repulsive forces, along with a collision avoidance algorithm, maintain safe inter-vehicular distances. The UAVs reach a stable formation equilibrium, after which the *Pre-Docking Phase* commences. Upon completion of the rendezvous procedure, the receivers disperse into positions behind the tanker aircraft as intended, each aligning with a designated refueling pod.

Summary of Results

In evaluating the performance of the UGV scenarios, the generated trajectories are found to be both collision-free and relatively direct, demonstrating efficient path planning. Moreover, the actual paths followed by the vehicles converge rapidly to the reference trajectories, indicating satisfactory tracking performance. This was demonstrated through comparisons of reference and actual trajectories, tracking error analysis through decaying plots and various metrics. On top of that control effort analysis has bolstered our claims for successful trajectory tracking performance. The primary area requiring improvement is the behavior of u_2, which exhibits large magnitudes and significant jitter throughout the operation.

In contrast to ground vehicles, the more complex dynamics of fixed-wing UAVs pose greater challenges for tracking control. The primary contribution of this work lies in high-level trajectory planning for multi-vehicle systems. Analysis of the generated

reference trajectories for the UAVs indicates that they are both safe and efficient, thereby achieving the central objective of this study.

When evaluating tracking performance along individual coordinate axes, the x-axis shows strong accuracy. The z-axis (altitude) exhibits some deviation, but the error gradually decreases over time. Given the physical scale and inherently slow dynamics of fixed-wing aircraft, this level of performance is considered acceptable. The y-axis, as previously discussed, shows a steady-state error due to lag in the direction of motion, a known and expected outcome under the current control framework.

To keep the implementation manageable, simplified dynamic models were used for the UAVs. While this allowed us to focus on trajectory generation, it also introduced limitations in tracking performance that could be improved in future work. Overall, the simulation results demonstrate that the proposed methods enable coordinated UAV behavior that meets mission objectives. Nevertheless, further refinements are possible to enhance system performance.

6. CONCLUSION AND FUTURE WORK

The primary objective of this work was to investigate the rendezvous phase of aerial refueling in a multi-UAV system. The rendezvous problem was addressed in two main stages: trajectory generation and trajectory tracking.

For trajectory generation, we employed virtual spring forces to simulate attraction between the target and the vehicles. To prevent collisions, the vehicles were modeled as particles with like electrical charges, causing mutual repulsion and thus discouraging clustering. These combined forces enabled the generation of reference trajectories that were both efficient and relatively safe. However, these methods do not guarantee collision-free paths: first, because the repulsive and attractive forces can balance each other out and still result in collisions, and second, because tracking deviations can cause vehicles to diverge from the safe reference trajectory and potentially collide.

To address this, we developed a novel collision avoidance algorithm inspired by road traffic etiquette. When a potential collision is detected, the trailing vehicle slows down, allowing the other vehicle to proceed. This is implemented by reducing the spring coefficient of the trailing vehicle. Additionally, a non-linear spring coefficient was introduced, which varies with the distance from the target, enhancing flexibility and control.

We validated the proposed techniques through numerical simulations. The trajectory generation approach produced successful results, and the distributed motion controllers developed for each vehicle yielded satisfactory tracking performance. Building on the 2D success, we extended the framework to a more realistic scenario involving fixed-wing UAVs in 3D space. Applying the same principles, we achieved promising results: UAVs initialized from arbitrary positions successfully navigated to predefined positions relative to the tanker aircraft, thus completing the rendezvous phase and preparing for the refueling procedure.

While this work focused on a specific application, the developed methods have broader applicability. Potential use cases include tracking dynamic targets, multi-

agent gathering and rendezvous missions, automated battery replacement for quadrotors, returning from missions to static bases, and general-purpose payload delivery or retrieval tasks—such as transporting medical supplies, ammunition, or fire extinguishing chemicals.

As for future work, the next logical step is to implement and validate the proposed methods on physical hardware. Therefore, the ultimate goal is to conduct real-world experimentation. Additionally, the environments considered in this work were highly idealized to facilitate the development and demonstration of the core concepts. To enable successful real-world deployment, these concepts must be tested in more realistic scenarios that include environmental disturbances and uncertainties.

BIBLIOGRAPHY

507th arw refuels thirsty rimpac aircraft [online image]. https://www.507arw.afrc.af.mil/News/Article-Display/Article/168946/507th-arw-refuels-thirsty-rimpac-aircraft/. Accessed: May 2025.

Aerial refueling: Examining the top 5 tanker aircraft [online image]. https://simpleflying.com/top-tanker-aircraft-list/. Accessed: May 2025.

Air to air refuelling – key force multiplier [online image]. https://australianairpowertoday.com.au/air-to-air-refuelling-key-force-multiplier/. Accessed: May 2025.

How aerial refueling works for military aircraft [online image]. https://aeroreport.de/en/good-to-know/how-aerial-refueling-works-for-military-aircraft. Accessed: May 2025.

Quantity and variety of russian il-78 [online image]. https://en.defence-ua.com/events/what_is_the_il_78_tanker_and_how_it_helps_kinzhal_carrying_mig_31k_stay_in_the_air_for_hours_straight-8724.html. Accessed: May 2025.

Abeywickrama, H. V., Jayawickrama, B. A., He, Y., & Dutkiewicz, E. (2017). Algorithm for energy efficient inter-uav collision avoidance. In *2017 17th International Symposium on Communications and Information Technologies (ISCIT)*, (pp. 1–5).

Abeywickrama, H. V., Jayawickrama, B. A., He, Y., & Dutkiewicz, E. (2018). Potential field based inter-uav collision avoidance using virtual target relocation. In *2018 IEEE 87th Vehicular Technology Conference (VTC Spring)*, (pp. 1–5).

Anderson, B. D. O., Fidan, B., Yu, C., & Walle, D. (2008a). Uav formation control: Theory and application. In Blondel, V. D., Boyd, S. P., & Kimura, H. (Eds.), *Recent Advances in Learning and Control*, (pp. 15–33)., London. Springer London.

Anderson, B. D. O., Fidan, B., Yu, C., & Walle, D. (2008b). Uav formation control: Theory and application. In Blondel, V. D., Boyd, S. P., & Kimura, H. (Eds.), *Recent Advances in Learning and Control*, (pp. 15–33)., London. Springer London.

Baras, J., Tan, X., & Hovareshti, P. (2003). Decentralized control of autonomous vehicles. In *42nd IEEE International Conference on Decision and Control (IEEE Cat. No.03CH37475)*, volume 2, (pp. 1532–1537 Vol.2).

Bishop, B. (2002). Behavior-based robotics: Ronald c. arkin; the mit press, cambridge, ma, 1998. *Automatica*, *38*, 2193–2196.

bo Chen, Y., chen Luo, G., song Mei, Y., qiao Yu, J., & long Su and, X. (2016). Uav path planning using artificial potential field method updated by optimal control theory. *International Journal of Systems Science*, *47*(6), 1407–1420.

Borkowski, A., Gnatowski, M., & Malec, J. (2001). Mobile robot cooperation in simple environments. In *Proceedings of the Second International Workshop on Robot Motion and Control. RoMoCo'01 (IEEE Cat. No.01EX535)*, (pp. 109–114).

Budiyanto, A., Cahyadi, A., Adji, T. B., & Wahyunggoro, O. (2015). Uav obstacle avoidance using potential field under dynamic environment. In *2015 Interna-*

tional Conference on Control, Electronics, Renewable Energy and Communications (ICCEREC), (pp. 187–192).

Cai, G., Lum, K.-Y., Chen, B. M., & Lee, T. H. (2010). A brief overview on miniature fixed-wing unmanned aerial vehicles. In *IEEE ICCA 2010*, (pp. 285–290).

Cao, Y., Yu, W., Ren, W., & Chen, G. (2013). An overview of recent progress in the study of distributed multi-agent coordination. *IEEE Transactions on Industrial Informatics*, *9*(1), 427–438.

Cook, K. L. B. (2007). The silent force multiplier: The history and role of uavs in warfare. In *2007 IEEE Aerospace Conference*, (pp. 1–7).

Cui, R., Ge, S. S., How, B. V. E., & Choo, Y. S. (2009). Leader-follower formation control of underactuated auvs with leader position measurement. In *2009 IEEE International Conference on Robotics and Automation*, (pp. 979–984).

Dalamagkidis, K., Valavanis, K. P., & Piegl, L. A. (2012). *Aviation History and Unmanned Flight*, (pp. 11–42). Dordrecht: Springer Netherlands.

Ding, X. C., Rahmani, A. R., & Egerstedt, M. (2010). Multi-uav convoy protection: An optimal approach to path planning and coordination. *IEEE Transactions on Robotics*, *26*(2), 256–268.

Duan, H., Yuan, Y., & Zeng, Z. (2022). Distributed cooperative control of multiple uavs in the presence of actuator faults and input constraints. *IEEE Transactions on Circuits and Systems II: Express Briefs*, *69*, 1–1.

Fang, Y., Yao, Y., Zhu, F., & Chen, K. (2023). Piecewise-potential-field-based path planning method for fixed-wing uav formation. *Scientific Reports*, *13*(5), 1–5.

Hao, G., Lv, Q., Huang, Z., Zhao, H., & Chen, W. (2023). Uav path planning based on improved artificial potential field method. *Aerospace*, *10*(6).

Hao, L. & Quan, Q. (2021). Autonomous aerial refueling of multiple uavs: An efficient rendezvous scheduling approach. In *2021 China Automation Congress (CAC)*, (pp. 7463–7468).

Huang, H., Zhou, H., Zheng, M., Xu, C., Zhang, X., & Xiong, W. (2019). Cooperative collision avoidance method for multi-uav based on kalman filter and model predictive control. In *2019 IEEE International Conference on Unmanned Systems and Artificial Intelligence (ICUSAI)*, (pp. 1–7).

Jaiswal, K. & Vashisth, A. (2023). A comprehensive analysis of uav collision avoidance techniques for enhanced aerial safety. In *2023 4th International Conference on Computation, Automation and Knowledge Management (ICCAKM)*, (pp. 1–6).

Jia, Q. & Li, G. (2007). Formation control and obstacle avoidance algorithm of multiple autonomous underwater vehicles(auvs) based on potential function and behavior rules. In *2007 IEEE International Conference on Automation and Logistics*, (pp. 569–573).

Lalish, E., Morgansen, K. A., & Tsukamaki, T. (2006). Formation tracking control using virtual structures and deconfliction. In *Proceedings of the 45th IEEE Conference on Decision and Control*, (pp. 5699–5705).

Lin, J., Morse, A., & Anderson, B. (2003). The multi-agent rendezvous problem. In *42nd IEEE International Conference on Decision and Control (IEEE Cat. No.03CH37475)*, volume 2, (pp. 1508–1513 Vol.2).

LIN, P., HE, Y., & CHEN, Y. (2024). Unmanned autonomous air-to-air refueling intelligent docking technology. *Chinese Journal of Aeronautics*, *37*(5), 1–5.

Loizou, S., Tanner, H., Kumar, V., & Kyriakopoulos, K. (2003). Closed loop motion planning and control for mobile robots in uncertain environments. In *42nd IEEE International Conference on Decision and Control (IEEE Cat. No.03CH37475)*, volume 3, (pp. 2926–2931 Vol.3).

Martínez, C., Richardson, T., Thomas, P., du Bois, J. L., & Campoy, P. (2013). A vision-based strategy for autonomous aerial refueling tasks. *Robotics and Autonomous Systems*, *61*(8), 876–895.

Mishra, D. P., Yadav, P., Rath, A., & Kumar, G. (2024). Advancements in obstacle avoidance technology for unmanned aerial vehicles (uavs). In *2024 1st International Conference on Cognitive, Green and Ubiquitous Computing (IC-CGU)*, (pp. 1–7).

Monteiro, S. & Bicho, E. (2002). A dynamical systems approach to behavior-based formation control. In *Proceedings 2002 IEEE International Conference on Robotics and Automation (Cat. No.02CH37292)*, volume 3, (pp. 2606–2611 vol.3).

Muskardin, T., Coelho, A., Noce, E. R. D., Ollero, A., & Kondak, K. (2020). Energy-based cooperative control for landing fixed-wing uavs on mobile platforms under communication delays. *IEEE Robotics and Automation Letters*, *5*(4), 5081–5088.

Muslimov, T. Z. & Munasypov, R. A. (2021). Consensus-based cooperative control of parallel fixed-wing uav formations via adaptive backstepping. *Aerospace Science and Technology*, *109*, 106416.

Nalepka, J. & Hinchman, J. (2005). *Automated Aerial Refueling: Extending the Effectiveness of UAVs*.

Ouyang, Q., Wu, Z., Cong, Y., & Wang, Z. (2023). Formation control of unmanned aerial vehicle swarms: A comprehensive review. *Asian Journal of Control*, *25*(1), 570–593.

Pan, Z., Zhang, C., Xia, Y., Xiong, H., & Shao, X. (2022). An improved artificial potential field method for path planning and formation control of the multi-uav systems. *IEEE Transactions on Circuits and Systems II: Express Briefs*, *69*(3), 1129–1133.

Paul, T., Krogstad, T. R., & Gravdahl, J. T. (2008). Uav formation flight using 3d potential field. In *2008 16th Mediterranean Conference on Control and Automation*, (pp. 1240–1245).

PS, R., . J. M. L. (2020). Mini unmanned aerial systems (uav) - a review of the parameters for classification of a mini uav. *International Journal of Aviation, Aeronautics, and Aerospace*, *7*(3), 1–5.

Rao, S. & Ghose, D. (2014). Sliding mode control-based autopilots for leaderless consensus of unmanned aerial vehicles. *IEEE Transactions on Control Systems Technology*, *22*(5), 1964–1972.

REN, J. & QUAN, Q. (2024). Progress in modeling and control of probe-and-drogue autonomous aerial refueling. *Chinese Journal of Aeronautics*, *37*(5), 6–26.

Ren, W. & Beard, R. (2003). A decentralized scheme for spacecraft formation flying via the virtual structure approach. In *Proceedings of the 2003 American Control Conference, 2003.*, volume 2, (pp. 1746–1751).

Samad, A. M., Kamarulzaman, N., Hamdani, M. A., Mastor, T. A., & Hashim, K. A. (2013). The potential of unmanned aerial vehicle (uav) for civilian and mapping application. In *2013 IEEE 3rd International Conference on System*

Engineering and Technology, (pp. 313–318).

Shao, Z., Yan, F., Zhou, Z., & Zhu, X. (2019). Path planning for multi-uav formation rendezvous based on distributed cooperative particle swarm optimization. *Applied Sciences*, *9*(13).

Sheng, W., Yang, Q., Tan, J., & Xi, N. (2004). Risk and efficiency: a distributed bidding algorithm for multi-robot coordination. In *Fifth World Congress on Intelligent Control and Automation (IEEE Cat. No.04EX788)*, volume 5, (pp. 4671–4675 Vol.5).

Spletzer, J., Das, A., Fierro, R., Taylor, C., Kumar, V., & Ostrowski, J. (2001). Cooperative localization and control for multi-robot manipulation. In *Proceedings 2001 IEEE/RSJ International Conference on Intelligent Robots and Systems. Expanding the Societal Role of Robotics in the the Next Millennium (Cat. No.01CH37180)*, volume 2, (pp. 631–636 vol.2).

Sullivan, J. (2006). Evolution or revolution? the rise of uavs. *IEEE Technology and Society Magazine*, *25*(3), 43–49.

Sun, Y., Chen, W., & Lv, J. (2022). Uav path planning based on improved artificial potential field method. In *2022 International Conference on Computer Network, Electronic and Automation (ICCNEA)*, (pp. 95–100).

van den Broek, T. H., van de Wouw, N., & Nijmeijer, H. (2009). Formation control of unicycle mobile robots: a virtual structure approach. In *Proceedings of the 48h IEEE Conference on Decision and Control (CDC) held jointly with 2009 28th Chinese Control Conference*, (pp. 8328–8333).

Vlantis, P., Vrohidis, C., Bechlioulis, C. P., & Kyriakopoulos, K. J. (2018). Robot navigation in complex workspaces using harmonic maps. In *2018 IEEE International Conference on Robotics and Automation (ICRA)*, (pp. 1726–1731).

Wu, C., Hui, J., Yan, J., Guo, Y., & Xiao, B. (2021). Dynamic modeling and faster finite-time attitude stabilization of receiver aircraft for aerial refueling. *Nonlinear Dynamics*, *104*.

Wu, X., Wang, F., & Qi, S. (2022). Unmanned autonomous aerial refueling control strategy design and test evaluation. In *2022 IEEE International Conference on Unmanned Systems (ICUS)*, (pp. 647–652).

Xiaoning, Z. (2020). Analysis of military application of uav swarm technology. In *2020 3rd International Conference on Unmanned Systems (ICUS)*, (pp. 1200–1204).

Yan, J., Yu, Y., & Wang, X. (2022). Distance-based formation control for fixed-wing uavs with input constraints: A low gain method. *Drones*, *6*(7).

Yan, Z., Jouandeau, N., & Cherif, A. A. (2013). A survey and analysis of multi-robot coordination. *International Journal of Advanced Robotic Systems*, *10*(12), 399.

Zhang, J., Yan, J., & Zhang, P. (2018). Fixed-wing uav formation control design with collision avoidance based on an improved artificial potential field. *IEEE Access*, *6*, 78342–78351.

Zhang, J., Yan, J., & Zhang, P. (2020). Multi-uav formation control based on a novel back-stepping approach. *IEEE Transactions on Vehicular Technology*, *69*(3), 2437–2448.

Zhou, Y., Rao, B., & Wang, W. (2020). Uav swarm intelligence: Recent advances and future trends. *IEEE Access*, *8*, 183856–183878.